S. Bennati, P. Fisicaro, P.S. Valvo. Meccanica (2013) 48:443–462.

doi: http://dx.doi.org/10.1007/s11012-012-9686-3

An enhanced beam-theory model of the mixed-mode bending (MMB) test – Part I: literature review and mechanical model

Stefano Bennati · Paolo Fisicaro · Paolo S. Valvo

Dipartimento di Ingegneria Civile e Industriale, Università di Pisa, Largo Lucio Lazzarino, 56126 Pisa, Italy

Phone +39 050 2218200

Fax +39 050 2218201

E-mail p.valvo@ing.unipi.it

Abstract The paper presents a mechanical model of the mixed-mode bending (MMB) test used to assess the mixed-mode interlaminar fracture toughness of composite laminates. The laminated specimen is considered as an assemblage of two sublaminates partly connected by an elastic–brittle interface. The problem is formulated through a set of 36 differential equations, accompanied by suitable boundary conditions. Solution of the problem is achieved by separately considering the two subproblems related to the symmetric and antisymmetric parts of the loads, which for symmetric specimens correspond to fracture modes I and II, respectively. Explicit expressions are determined for the interfacial stresses, internal forces, and displacements.

Keywords *Mixed-mode bending (MMB) test · Beam-theory model · Analytical solution · Laminated composite · Interlaminar fracture toughness · Delamination*

1 Introduction

Delamination, or interlaminar fracture, is a major failure mode for fibre-reinforced composite laminates. A vast body of literature is available on this subject (see the reviews by Garg [1], Sela and Ishai [2], and Tay [3]). The phenomenon is commonly analysed within the context of Fracture Mechanics, where the onset and growth of delaminations are predicted according to criteria based on the energy release rate, G [4]. Specific laboratory tests have been developed to assess delamination toughness under pure (I or opening, II or sliding, and III or tearing) and mixed fracture modes [5, 6]. In particular, for I/II mixed-mode fracture, the *mixed-mode bending* (MMB) test, introduced by Reeder and Crews in 1988 [7, 8], was adopted, after some refinements [9–12], as an ASTM standard in 2001 (updated in 2006 [13]). This test method soon gained great popularity because it allows a wide range of mode mixities to be characterised using a single specimen geometry. In addition, by assuming a linear mechanical model, the MMB test can be regarded as the superposition of the *double cantilever beam* (DCB) and *end-notched flexure* (ENF) tests. Thus, the models developed for the latter tests can be exploited to interpret the results of the MMB test, in particular, to determine the modal contributions to the energy release rate, G_I and G_{II}. On the other hand, one drawback to this test method is the complexity and cost of the testing apparatus as compared to alternative, simpler mixed-mode test procedures [6].

We present an *enhanced beam-theory* (EBT) model of the MMB test, wherein the laminated specimen is considered as an assemblage of two sublaminates partly connected by a deformable interface. The sublaminates are modelled as extensible, flexible, and shear-deformable beams, according to Timoshenko's theory. The interface is regarded as a continuous distribution of linearly elastic–brittle springs acting along the normal and tangential directions with respect to the interface plane. Thus, both normal and tangential stresses are exchanged through the interface, and the sublaminates are subjected to distributed axial load, distributed transverse load, and distributed couple. Our modelling approach dates back to the pioneering work on interface models by Allix and Ladevèze [14] and Corigliano [15], amongst others, and has already been successfully adopted for modelling the *asymmetric double cantilever beam* (ADCB) test [16].

The behaviour of the mechanical model is described by a set of 36 differential equations, endowed with suitable boundary conditions. The differential problem is solved assuming that the following hypotheses are fulfilled:

a) the delamination is placed at the mid-plane of the specimen, which is split into two sublaminates having same mechanical properties;
b) the sublaminates behave as plane beams and exhibit neither shear-extension nor bending-extension coupling;
c) non-linear effects are negligible.

Solution of the problem is achieved through the superposition principle by separately considering the two subproblems related to the symmetric and antisymmetric parts of the loads, which for symmetric specimens correspond to fracture modes I (opening) and II (sliding), respectively. Then, explicit expressions for the interfacial stresses, internal forces, and displacements are determined. By way of illustration, plots of the abovementioned quantities are furnished for the case of a unidirectional laminated MMB test specimen. It should however be stressed that the analytical solution obtained holds for both unidirectional and multidirectional specimens, as well as for adhesively bonded specimens.

In Part II of this paper analytical expressions will be deduced for the compliance, energy release rate, and mode mixity. Comparisons will also be presented with some analytical models reported in the literature and finite element analyses carried out to this end. Lastly, some examples of unidirectional and multidirectional laminates will serve to illustrate use of the proposed model for experimental data reduction [17].

2 The mixed-mode bending test: test description and literature review

The MMB test (Fig. 1) is basically a bending test carried out on a (unidirectional) laminated specimen affected by a pre-implanted delamination at one of its ends. The specimen has width B (not shown in the figure) and thickness H, and is simply supported over a span of length L. The delamination splits the laminate into two sublaminates of equal thickness, $h = H/2$. We denote with a the effective delamination length (measured between the left-hand end support and the crack tip) and with $b = L - a$ the length of the unbroken part of the specimen (measured between the crack tip and the right-hand end support).

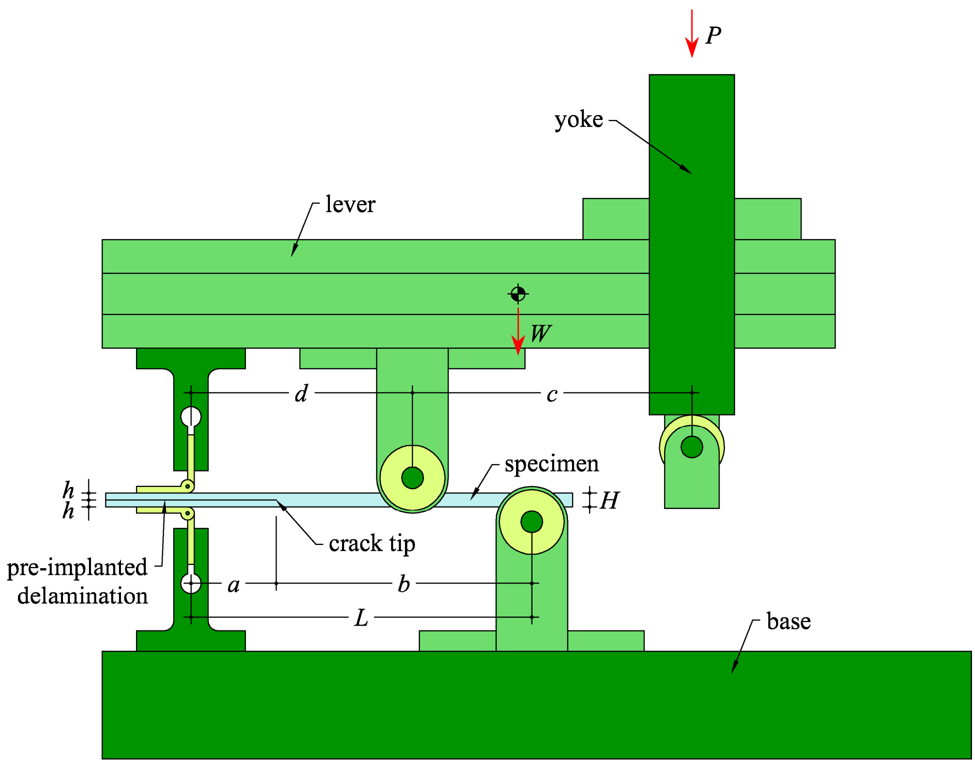

Fig. 1 MMB testing apparatus

The specimen is loaded indirectly through a lever of weight W, to which the testing machine applies a variable load, P. The resultant force, $R = P + W$, is transferred to the specimen as an upward load, P_u, and a downward load, P_d (Fig. 2). Equilibrium of the lever shows that

$$P_u = \frac{c}{d} P + \frac{c_W}{d} W \quad \text{and} \quad P_d = (1 + \frac{c}{d}) P + (1 + \frac{c_W}{d}) W \,, \tag{1}$$

where c and d are the lengths of the lever arms, c_W is the distance of the lever's centre of gravity from the application point of P_d (see Reeder [11] and Chen *et al.* [18] for a discussion on the effects of the lever's weight on test results).

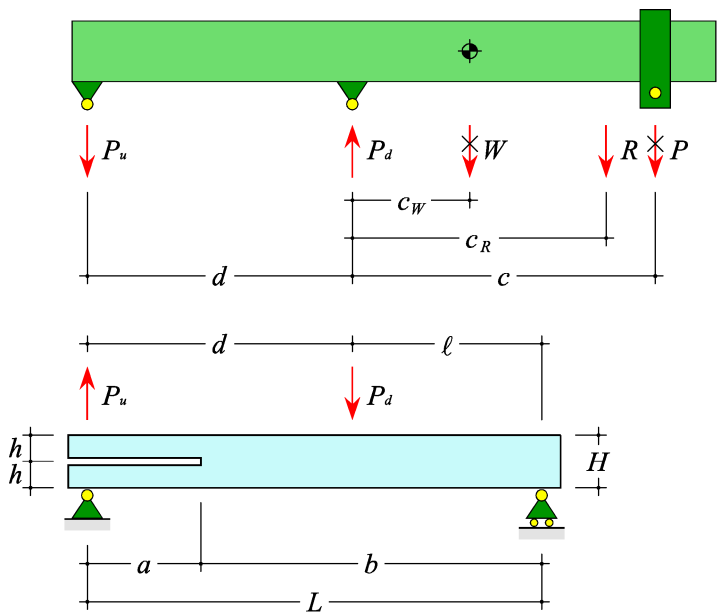

Fig. 2 Scheme of the loading lever and specimen

The lever arm lengths, c and d, can be adjusted to vary the intensities of P_u and P_d and, consequently, impose a desired I/II mixed-mode ratio, $\alpha = G_{\mathrm{I}} / G_{\mathrm{II}}$. The original test procedure [7, 8] (now accepted as an ASTM standard [13]) fixes the length $d = L/2$ and allows only c to be varied. The range of mode mixities thus obtainable has a practical upper limit (related to the length of the lever). To overcome this limit, Kinloch *et al.* [19] proposed modifying the test procedure to also allow length d to be varied. This *modified MMB* test has since been considered by several Authors [20–24]. We also consider a general value of d. Furthermore, we define the length $\ell = L - d$ and recover the standard case by setting $d = \ell = L/2$.

By suitably decomposing the forces applied to the specimen, the MMB test can be regarded as the superposition of DCB (mode I) and ENF (mode II) tests (Fig. 3). Thus,

$$P_{\mathrm{I}} = P_u - \frac{\ell}{2L} P_d \quad \text{and} \quad P_{\mathrm{II}} = P_d \tag{2}$$

are the loads responsible for fracture modes I and II, respectively.

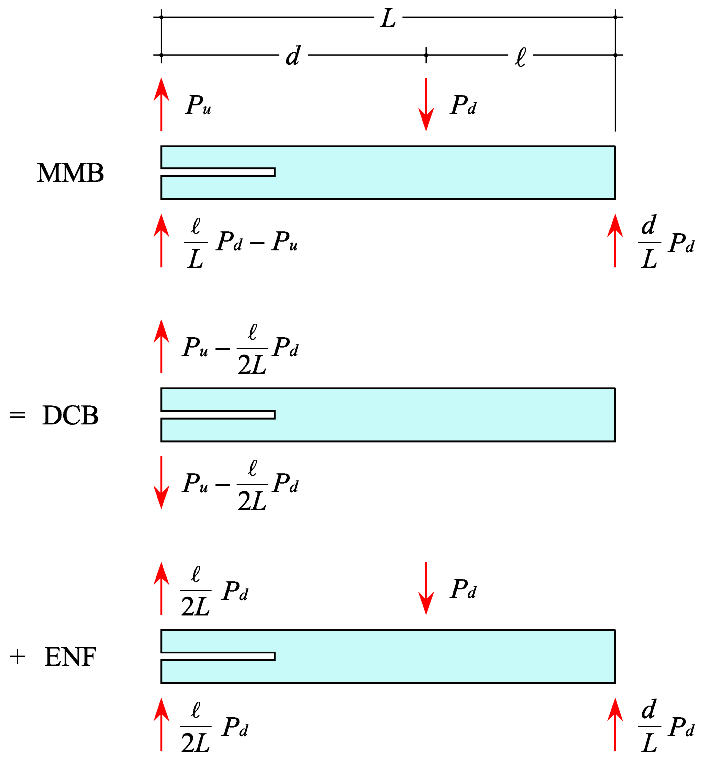

Fig. 3 MMB test as the superposition of DCB and ENF tests

For experimental data reduction, a theoretical model of the test is required [25]. To this end, a number of models of growing complexity have been proposed in the literature and are briefly recalled in the following. In the *simple beam-theory* (SBT) model [8], the specimen is considered as an assemblage of three rigidly connected beams made of a linearly elastic, homogenous isotropic material. The SBT model, however, suffers from some oversimplifying assumptions that lead to underestimation of compliance and energy release rate with respect to experimental and numerical results. Reeder and Crews [7, 8] have already made some suggestions as to how to improve the SBT model's predictions by introducing correction terms into the expressions for G_{I} and G_{II}. In particular, they considered the contributions stemming from Kanninen's elastic foundation model of the DCB test [26] and Timoshenko's shear-deformable beam theory. In this respect, however, it should be noted that their expression for G_{II} (derived from Carlsson *et al.* [27]) has recently been proved incorrect by Fan *et al.* [28] and Valvo [29].

Williams [30] showed how the effect of deflections and rotations at the crack tip included in Kanninen's model can be considered approximately by adding a correction term, χh, to the delamination length, a, where χ is a factor related to the elastic properties of the material. This *corrected beam theory* (CBT) model was extended to mode II delamination fracture by Hashemi *et al.* [31]. Wang and Williams [32] pointed out that distinct correction factors, χ_{I} and χ_{II}, should be used for fracture modes I and II, and Kinloch *et al.* [19] applied this modelling approach to the MMB test. The proposed *crack length correction parameters* are now included in the formulas for data reduction recommended by the ASTM standard [13]. These formulas, however, hold only for unidirectional laminated or homogeneous orthotropic specimens, and do not apply to laminates with generic stacking sequences. Moreover, the mode II crack length correction parameter is calculated simply as a fraction of the corresponding mode I parameter. In this regard, more accurate estimates for the mode II correction parameter have been recently given by Wang and Qiao [33], de Morais [34], and Jumel *et al.* [35].

Many Authors have considered multidirectional and asymmetric MMB test specimens. De Morais and Pereira have proposed applying the CBT model to multidirectional laminated specimens by calculating the crack length correction parameters based on the homogenised flexural and shear moduli [36–38]. For asymmetric specimens, they suggest using different crack length correction parameters for the upper and lower sublaminates [39]. Ducept *et al.* [40–42] studied specimens with asymmetric stacking sequences, by using the *compliance calibration method*, formerly proposed by Benzeggagh and Kenane [43] and Martin and Hansen [44]. Ozdil and Carlsson [45] and Kim and Mayer [46] studied angle-ply and cross-ply laminated specimens. Soboyejo *et al.* [22], Marannano and Pasta [23], Suàrez *et al.* [24], and Yokozeki *et al.* [47] analysed specimens where the delamination is located between sublaminates different for thickness or material. Jagan *et al.* [48] considered graded laminates, and Quispitupa *et al.* [49] analysed MMB sandwich specimens. In the case of asymmetric specimens, particular attention should be devoted to the partitioning of fracture modes, which cannot be achieved by simply considering the asymmetric MMB test as the superposition of asymmetric DCB and ENF tests. In fact, because of the asymmetry, both the asymmetric DCB and ENF tests turn out to be mixed-mode delamination tests. Unfortunately, with few exceptions [39, 41], this point appears not to have been fully appreciated in the literature [22–24, 36–38, 45–49]. Developing a mechanical model of the asymmetric MMB test is thus still an open issue.

In recent years, many alternative strategies have been proposed for the numerical analysis of the MMB test. Allix and Corigliano [50] implemented an interface law relating interlaminar stresses to displacement discontinuities. Miravete and Jiménez [51, 52] modelled the MMB test using solid finite elements and computed the energy release rate through the *virtual crack closure technique* (VCCT). Cohesive interface elements have been used in association with solid elements by Camanho *et al.* [53], Turon *et al.* [54], Tumino and Cappello [55], Oliveira *et al.* [56], and de Moura *et al.* [57]; with plane elements by Warrior *et al.* [58] and Iannucci [59]; and with shell elements by Borg *et al.* [60]. Aymerich *et al.* [61] and van der Meer and Sluys [62] have proposed new numerical strategies to model delamination and used the MMB test as a validation example.

Analytical models of the MMB test have also been proposed in more recent literature. Blanco *et al.* [63] present a formula for determining the lever arm length, c, as a function of the mode mixity. Tenchev and Falzon [64] analyse the case of a delamination propagating beyond the application point of P_d. Massabò and Cox [65] analyse an MMB test specimen with through-the-thickness reinforcements. Lastly, Szekrényes and Uj [66] and Szekrényes [67] have formulated an *improved beam-theory* (IBT) model, whereby the specimen is modelled as an assemblage of two Euler-Bernoulli beams connected by a Winkler–Pasternak foundation, consisting of extensional and rotational distributed springs, while the effects of transverse shear, crack tip shear deformation and root rotations are taken into account through several correction terms.

3 Formulation of the problem

3.1 Mechanical model

In the enhanced beam-theory model (Fig. 4), the MMB test specimen is regarded as made of two sublaminates of thickness h, connected by a deformable interface of thickness $t << h$. We introduce an abscissa, s, measuring the distance of the generic cross section from the crack tip. Two local reference systems, $O_1x_1z_1$ and $O_2x_2z_2$, are defined with their origins on the centrelines of the upper and lower sublaminates, respectively. Henceforth, index $i = 1$ refers to the upper sublaminate, index $i = 2$ to the lower sublaminate. Accordingly, we indicate with u_i and w_i the sublaminates' mid-plane displacements along the axial and transverse directions, respectively, and with ϕ_i their cross sections' rotations (positive if counter-clockwise).

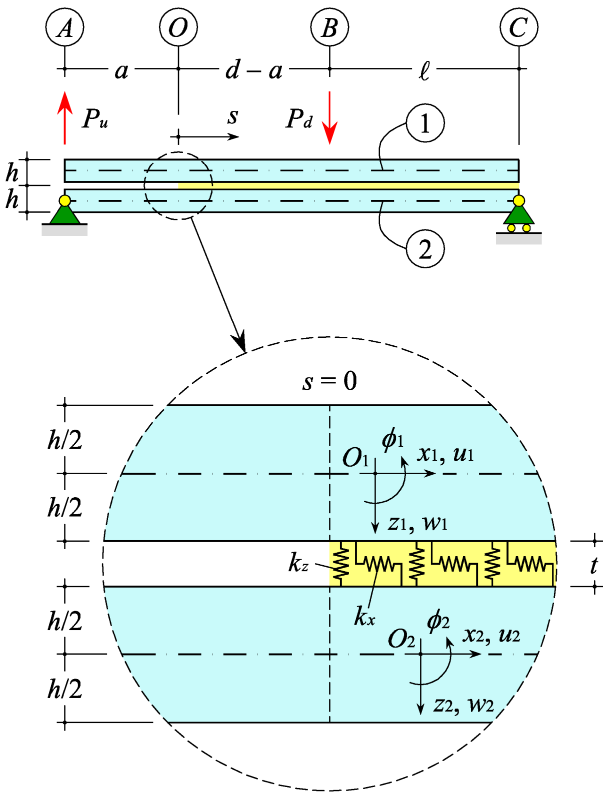

Fig. 4 Enhanced beam-theory model of the MMB test

We assume the two sublaminates have identical mechanical properties, so that in line with classical laminated plate theory [68], $A_1 = A_2$, $C_1 = C_2$, and $D_1 = D_2$ are the sublaminates' extensional stiffness, shear stiffness, and bending stiffness, respectively. The sublaminates may have any stacking sequence, provided that they behave as plane beams and exhibit neither shear-extension nor bending-extension coupling. Note that this condition is fulfilled not only by homogenous and unidirectional laminated specimens, but also by symmetric cross-ply and angle-ply specimens, as well as more general uncoupled multidirectional laminated specimens [69].

The constitutive laws for the sublaminates are

$$N_i = B\,A_i\varepsilon_i, \quad Q_i = B\,C_i\gamma_i, \quad \text{and} \quad M_i = B\,D_i\kappa_i, \tag{3}$$

where N_i, Q_i, and M_i are the axial force, shear force, and bending moment, and

$$\varepsilon_i = \frac{du_i}{ds}, \quad \gamma_i = \phi_i + \frac{dw_i}{ds}, \quad \text{and} \quad \kappa_i = \frac{d\phi_i}{ds} \tag{4}$$

are the axial strain, shear strain, and curvature [70], respectively.

The deformable interface is modelled as two independent, uniform distributions of elastic–brittle springs acting along the normal and tangential directions with respect to the interface plane. Accordingly, the normal and tangential interfacial stresses are

$$\sigma = k_z\,\Delta w \quad \text{and} \quad \tau = k_x\,\Delta u, \tag{5}$$

where k_z and k_x are the elastic constants of the interface and $\Delta w = \overline{w}_2 - \underline{w}_1$ and $\Delta u = \overline{u}_2 - \underline{u}_1$ are the transverse and axial relative displacements at the interface, respectively. Here, $\underline{u}_1$ and $\underline{w}_1$ are the displacements at the bottom surface ($z_1 = h/2$) of the upper sublaminate; $\overline{u}_2$ and $\overline{w}_2$ are the displacements at the top surface ($z_2 = -h/2$) of the lower sublaminate. According to beam-theory kinematics, the sublaminates' axial displacements vary linearly with the thickness coordinate, so that $\underline{u}_1 = u_1 + \phi_1\,h/2$ and $\overline{u}_2 = u_2 - \phi_2\,h/2$, while the transverse displacements are assumed to be constant throughout the thickness, so that $\underline{w}_1 = w_1$ and $\overline{w}_2 = w_2$. Hence,

$$\Delta u = u_2 - u_1 - \frac{h}{2}(\phi_1 + \phi_2) \quad \text{and} \quad \Delta w = w_2 - w_1. \tag{6}$$

By substituting Eqs. (6) into (5), we obtain

$$\sigma = k_z(w_2 - w_1) \quad \text{and} \quad \tau = k_x\,[u_2 - u_1 - \frac{h}{2}(\phi_1 + \phi_2)]\,. \tag{7}$$

3.2 Differential problem

The mechanical model is described by three sets of differential equations, corresponding to three intervals for the abscissa, *s*: interval $AO = [s_A, 0] = [-a, 0]$, ranging from the application point of P_u to the crack tip; interval $OB = [0, s_B] = [0, d-a]$, from the crack tip to the application point of P_d; interval $BC = [s_B, s_C] = [d-a, b]$, from the application point of P_d to the specimen's right-hand end support (Fig. 4).

Within interval *AO*, the upper and lower sublaminates do not exchange any distributed load, so that the equilibrium equations are simply

$$\frac{dN_i}{ds} = 0, \quad \frac{dQ_i}{ds} = 0, \quad \text{and} \quad \frac{dM_i}{ds} - Q_i = 0. \tag{8}$$

Instead, within intervals *OB* and *BC*, the two sublaminates are connected to each other by the interface, so that the equilibrium equations are

$$\frac{dN_i}{ds} + n_i = 0, \quad \frac{dQ_i}{ds} + q_i = 0, \quad \text{and} \quad \frac{dM_i}{ds} + m_i - Q_i = 0, \tag{9}$$

where

$$n_1 = -n_2 = B\tau, \quad q_1 = -q_2 = B\sigma, \quad \text{and} \quad m_1 = m_2 = B\tau h/2, \tag{10}$$

are the distributed axial load, distributed transverse load, and distributed couple, respectively. In Eqs. (10), the interfacial stresses, σ and τ, are given by Eqs. (7).

Finally, the displacements are introduced into the problem by substituting Eqs. (4) into (3) to yield

$$\frac{du_i}{ds} = \frac{N_i}{BA_i}, \quad \frac{dw_i}{ds} + \phi_i = \frac{Q_i}{BC_i}, \quad \text{and} \quad \frac{d\phi_i}{ds} = \frac{M_i}{BD_i}. \tag{11}$$

The differential problem stated by Eqs. (8)–(11) consists of 36 first-order differential equations (12 for each of the three intervals of the curvilinear abscissa) for the 36 unknown functions describing the internal forces and displacements. The problem is completed by 36 boundary conditions (21 static plus 15 kinematic), which are detailed in Appendix A.

4 Solution of the problem

4.1 Solution strategy

In order to tackle the stated differential problem, it is convenient to first solve Eqs. (8)–(10) in terms of the internal forces and, subsequently, integrate Eqs. (11) to deduce the displacements. In this way, however, the interfacial stresses have to be determined together with the internal forces. In order to introduce the interfacial stresses into the differential problem, we suitably differentiate Eqs. (7) with respect to s and substitute Eqs. (11) into the resulting expressions. Thus, we obtain

$$\begin{aligned} \frac{d\tau}{ds} &= \frac{k_x}{B}\left(\frac{N_2 - N_1}{A_1} - \frac{h}{2}\frac{M_1 + M_2}{D_1}\right), \\ \frac{d^2\sigma}{ds^2} &= \frac{k_z}{B}\left[\frac{1}{C_1}\left(\frac{dQ_2}{ds} - \frac{dQ_1}{ds}\right) - \frac{M_2 - M_1}{D_1}\right], \end{aligned} \tag{12}$$

which, together with Eqs. (8) and (9), compose a set of 20 first-order and 2 second-order differential equations for the internal forces and interfacial stresses.

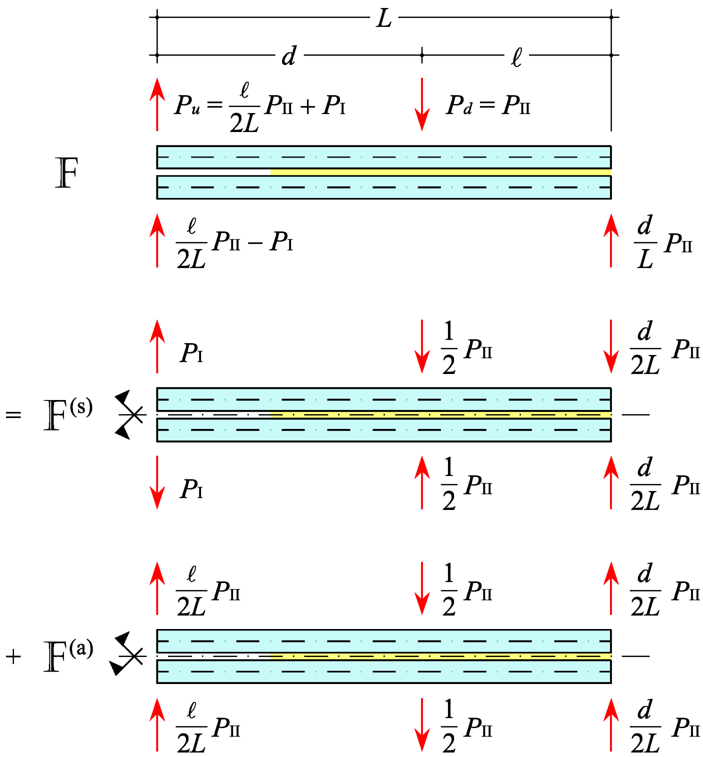

Fig. 5 Decomposition of the load system into symmetric and antisymmetric parts

Proceeding with the solution, we consider a free-body diagram of the specimen and compute the support reactions. Then, observing that the specimen is symmetric about its mid-plane, we decompose the actual load system into the sum of a symmetric load system plus an antisymmetric load system (Fig. 5). To this end, remembering Eqs. (2), it is convenient to express the upward and downward loads as

$$P_{\mathrm{u}} = P_{\mathrm{I}} + \frac{\ell}{2L} P_{\mathrm{II}} \quad \text{and} \quad P_{\mathrm{d}} = P_{\mathrm{II}} . \tag{13}$$

The solution for the original system, $\mathbb{F}$, can now be expressed as

$$\begin{aligned} &u_i = u_i^{(\mathrm{s})} + u_i^{(\mathrm{a})}, \quad && w_i = w_i^{(\mathrm{s})} + w_i^{(\mathrm{a})}, \quad && \phi_i = \phi_i^{(\mathrm{s})} + \phi_i^{(\mathrm{a})}, \\ &N_i = N_i^{(\mathrm{s})} + N_i^{(\mathrm{a})}, \quad && Q_i = Q_i^{(\mathrm{s})} + Q_i^{(\mathrm{a})}, \quad && M_i = M_i^{(\mathrm{s})} + M_i^{(\mathrm{a})}, \end{aligned} \tag{14}$$

and

$$\sigma = \sigma^{(\mathrm{s})} + \sigma^{(\mathrm{a})} \quad \text{and} \quad \tau = \tau^{(\mathrm{s})} + \tau^{(\mathrm{a})} . \tag{15}$$

Here (and henceforth), the superscripts (s) and (a) are used to refer to the solutions for the symmetric and antisymmetric systems, $\mathbb{F}^{(\mathrm{s})}$ and $\mathbb{F}^{(\mathrm{a})}$, respectively.

The solution to the symmetric subproblem must fulfil the symmetry conditions

$$\begin{aligned} &u_2^{(\mathrm{s})} = u_1^{(\mathrm{s})}, \quad && w_2^{(\mathrm{s})} = -w_1^{(\mathrm{s})}, \quad && \phi_2^{(\mathrm{s})} = -\phi_1^{(\mathrm{s})}, \\ &N_2^{(\mathrm{s})} = N_1^{(\mathrm{s})}, \quad && Q_2^{(\mathrm{s})} = -Q_1^{(\mathrm{s})}, \quad && M_2^{(\mathrm{s})} = -M_1^{(\mathrm{s})}; \end{aligned} \tag{16}$$

while the solution to the antisymmetric subproblem must satisfy

$$\begin{aligned} &u_2^{(\mathrm{a})} = -u_1^{(\mathrm{a})}, \quad && w_2^{(\mathrm{a})} = w_1^{(\mathrm{a})}, \quad && \phi_2^{(\mathrm{a})} = \phi_1^{(\mathrm{a})} \\ &N_2^{(\mathrm{a})} = -N_1^{(\mathrm{a})}, \quad && Q_2^{(\mathrm{a})} = Q_1^{(\mathrm{a})}, \quad && M_2^{(\mathrm{a})} = M_1^{(\mathrm{a})}. \end{aligned} \tag{17}$$

By substituting Eqs. (14)–(17) into (6)–(7), it immediately follows that

$$\Delta w^{(\mathrm{a})} = w_2^{(\mathrm{a})} - w_1^{(\mathrm{a})} = 0 \quad \Rightarrow \quad \sigma^{(\mathrm{a})} = 0 \tag{18}$$

and

$$\Delta u^{(\mathrm{s})} = u_2^{(\mathrm{s})} - u_1^{(\mathrm{s})} - \frac{h}{2}(\phi_1^{(\mathrm{s})} + \phi_2^{(\mathrm{s})}) = 0 \quad \Rightarrow \quad \tau^{(\mathrm{s})} = 0 ; \tag{19}$$

hence,

$$\sigma = \sigma^{(\mathrm{s})} = -2k_z w_1^{(\mathrm{s})} \quad \text{and} \quad \tau = \tau^{(\mathrm{a})} = -2k_x (u_1^{(\mathrm{a})} + \frac{h}{2}\phi_1^{(\mathrm{a})}) . \tag{20}$$

It is thus demonstrated that the symmetric load system produces only normal interfacial stresses, so it is related to pure mode I fracture; conversely, the antisymmetric load system is responsible only for tangential interfacial stresses, so it corresponds to pure mode II fracture. It is important to stress that such result does not hold if the specimen is not symmetric about its mid-plane.

4.2 Symmetric subproblem (mode I fracture)

4.2.1 Solution of the differential problem

Thanks to the symmetry conditions, in solving the symmetric subproblem, we can limit our analysis to the upper sublaminate (Fig. 6) and deduce the solution for the lower sublaminate from Eqs. (16).

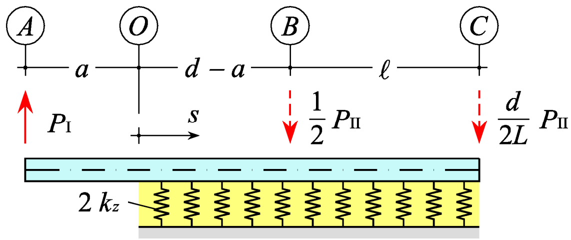

Fig. 6 Symmetric subproblem for the upper sublaminate

The differential equations for the upper sublaminate are

$$\frac{dN_1^{(s)}}{ds} = 0, \quad \frac{dQ_1^{(s)}}{ds} = 0, \quad \text{and} \quad \frac{dM_1^{(s)}}{ds} - Q_1^{(s)} = 0, \tag{21}$$

within interval AO, and

$$\begin{aligned} &\frac{dN_1^{(s)}}{ds} = 0, \quad \frac{dQ_1^{(s)}}{ds} + B\sigma^{(s)} = 0, \quad \frac{dM_1^{(s)}}{ds} - Q_1^{(s)} = 0, \\ &\frac{d^2\sigma}{ds^2} = \frac{2k_z}{B}\left(\frac{M_1^{(s)}}{D_1} - \frac{1}{C_1}\frac{dQ_1^{(s)}}{ds}\right), \end{aligned} \tag{22}$$

within intervals OB and BC. From Eqs. (21) it is a straightforward matter to obtain the internal forces in interval AO,

$$N_1^{(s)} = A_1, \quad Q_1^{(s)} = A_2, \quad \text{and} \quad M_1^{(s)} = A_2 s + A_3, \tag{23}$$

where A_1, A_2, and A_3 are integration constants. Moving on to solve Eqs. (22), we immediately find the axial force,

$$N_1^{(s)} = B_1, \tag{24}$$

where B_1 is an integration constant. Then, by substituting the second and third equations in (22) into the fourth one, we obtain a fourth-order differential equation,

$$\frac{d^4 M_1^{(s)}}{ds^4} - \frac{2k_z}{C_1}\frac{d^2 M_1^{(s)}}{ds^2} + \frac{2k_z}{D_1} M_1^{(s)} = 0\,, \tag{25}$$

for the bending moment. Its biquadratic characteristic equation,

$$\lambda^4 - \frac{2k_z}{C_1}\lambda^2 + \frac{2k_z}{D_1} = 0\,, \tag{26}$$

has the following four roots:

$$\begin{aligned} &\lambda_1 = \sqrt{\frac{k_z}{C_1}\left(1+\sqrt{1-\frac{2\,C_1^2}{k_z D_1}}\right)}, \quad && \lambda_2 = \sqrt{\frac{k_z}{C_1}\left(1-\sqrt{1-\frac{2\,C_1^2}{k_z D_1}}\right)}, \\ &\lambda_3 = -\lambda_1, && \lambda_4 = -\lambda_2. \end{aligned} \tag{27}$$

Provided that $\lambda_1 \neq \lambda_2$ (which excludes the case $k_z = k_z^* = 2\,C_1^{\,2} / D_1$, for which the solution must therefore be deduced separately), the bending moment can be written as

$$M_1^{(s)} = B_2 \cosh \lambda_1 s + B_3 \sinh \lambda_1 s + B_4 \cosh \lambda_2 s + B_5 \sinh \lambda_2 s\,, \tag{28}$$

where B_2, B_3, B_4, and B_5 are integration constants. From the third equation in (22) we obtain the shear force,

$$Q_1^{(s)} = \lambda_1 (B_2 \sinh \lambda_1 s + B_3 \cosh \lambda_1 s) + \lambda_2 (B_4 \sinh \lambda_2 s + B_5 \cosh \lambda_2 s)\,, \tag{29}$$

and from the second equation in (22), the normal interfacial stress,

$$\sigma = -\frac{1}{B}[\lambda_1^2 (B_2 \cosh \lambda_1 s + B_3 \sinh \lambda_1 s) + \lambda_2^2 (B_4 \cosh \lambda_2 s + B_5 \sinh \lambda_2 s)]\,. \tag{30}$$

4.2.2 Static boundary conditions

The boundary conditions for the problem at hand should rigorously take into account the presence of concentrated loads in sections B and C (Fig. 6). These loads correspond in the full specimen (Fig. 5) to transverse compressive forces, transferred from one sublaminate to the other through the interface. However, it can be shown that for common composite laminates this load transfer is localised within very narrow regions and the effects on the specimen's compliance and energy release rate are extremely limited. Therefore, in the present solution we disregard these loads, thus avoiding the resulting complications (both analytical and numerical) of little interest for practical purposes.

The eight unknown integration constants are determined by imposing the following boundary conditions:

$$\begin{aligned}
&N_1^{(s)}\Big|_{s=s_A} = 0, && Q_1^{(s)}\Big|_{s=s_A} = P_{\mathrm{I}}, && M_1^{(s)}\Big|_{s=s_A} = 0, \\
&N_1^{(s)}\Big|_{s=0^-} = N_1^{(s)}\Big|_{s=0^+}, && Q_1^{(s)}\Big|_{s=0^-} = Q_1^{(s)}\Big|_{s=0^+}, && M_1^{(s)}\Big|_{s=0^-} = M_1^{(s)}\Big|_{s=0^+}, \\
& && Q_1^{(s)}\Big|_{s=s_C} = 0, && M_1^{(s)}\Big|_{s=s_C} = 0.
\end{aligned} \tag{31}$$

By substituting the expressions for the internal forces deduced in Section 4.2.1 into Eqs. (31), the integration constants are determined as follows:

$$\begin{aligned}
&A_1 = 0, \quad A_2 = P_{\mathrm{I}}, \quad A_3 = aP_{\mathrm{I}}, \\
&B_1 = 0, \quad B_2 = b_2 P_{\mathrm{I}}, \quad B_3 = b_3 P_{\mathrm{I}}, \quad B_4 = b_4 P_{\mathrm{I}}, \quad B_5 = b_5 P_{\mathrm{I}},
\end{aligned} \tag{32}$$

where

$$b_2 = -\frac{\beta_1 + \lambda_2 a \beta_2}{\beta_0}, \quad b_3 = \frac{\beta_3 + \lambda_2 a \beta_4}{\beta_0}, \quad b_4 = \frac{\beta_1 + \lambda_1 a \beta_3}{\beta_0}, \quad b_5 = -\frac{\beta_2 + \lambda_1 a \beta_4}{\beta_0} \tag{33}$$

and

$$\begin{aligned}
&\beta_0 = (\lambda_1^2 + \lambda_2^2)\tanh \lambda_1 b \tanh \lambda_2 b - 2\lambda_1\lambda_2(1 - \operatorname{sech} \lambda_1 b \operatorname{sech} \lambda_2 b), \\
&\beta_1 = \lambda_1 \tanh \lambda_2 b - \lambda_2 \tanh \lambda_1 b, \\
&\beta_2 = \lambda_1 (1 - \operatorname{sech} \lambda_1 b \operatorname{sech} \lambda_2 b) - \lambda_2 \tanh \lambda_1 b \tanh \lambda_2 b, \\
&\beta_3 = \lambda_1 \tanh \lambda_1 b \tanh \lambda_2 b - \lambda_2 (1 - \operatorname{sech} \lambda_1 b \operatorname{sech} \lambda_2 b), \\
&\beta_4 = \lambda_1 \tanh \lambda_1 b - \lambda_2 \tanh \lambda_2 b.
\end{aligned} \tag{34}$$

4.2.3 Internal forces and interfacial stresses

By substituting the expressions for the integration constants (32) into the solution to the differential problem deduced in Section 4.2.1, we obtain the internal forces

$$N_1^{(s)} = 0, \quad Q_1^{(s)} = P_{\mathrm{I}}, \quad \text{and} \quad M_1^{(s)} = P_{\mathrm{I}}(s + a), \tag{35}$$

within interval AO; and the internal forces and interfacial stresses

$$
\begin{aligned}
&N_1^{(s)} = 0,\\
&Q_1^{(s)} = P_{\mathrm{I}}\,[\lambda_1(b_2 \sinh \lambda_1 s + b_3 \cosh \lambda_1 s) + \lambda_2(b_4 \sinh \lambda_2 s + b_5 \cosh \lambda_2 s)],\\
&M_1^{(s)} = P_{\mathrm{I}}\,(b_2 \cosh \lambda_1 s + b_3 \sinh \lambda_1 s + b_4 \cosh \lambda_2 s + b_5 \sinh \lambda_2 s),\\
&\sigma = -\frac{P_{\mathrm{I}}}{B}[\lambda_1^2(b_2 \cosh \lambda_1 s + b_3 \sinh \lambda_1 s) + \lambda_2^2(b_4 \cosh \lambda_2 s + b_5 \sinh \lambda_2 s)],
\end{aligned}
\tag{36}
$$

within intervals OB and BC.

4.3 Antisymmetric subproblem (mode II fracture)

4.3.1 Solution of the differential problem

Thanks to the antisymmetry conditions, in solving the antisymmetric subproblem we can limit our analysis to the upper sublaminate (Fig. 7) and deduce the solution for the lower sublaminate from Eqs. (17).

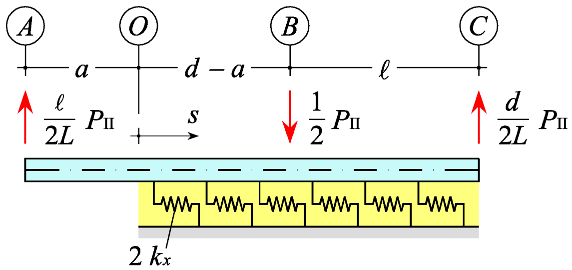

Fig. 7 Antisymmetric subproblem for the upper sublaminate

The differential equations for the upper sublaminate are

$$
\frac{dN_1^{(a)}}{ds} = 0, \quad \frac{dQ_1^{(a)}}{ds} = 0, \quad \text{and} \quad \frac{dM_1^{(a)}}{ds} - Q_1^{(a)} = 0\,,
\tag{37}
$$

within interval AO, and

$$
\begin{aligned}
&\frac{dN_1^{(a)}}{ds} + B\tau = 0, \quad \frac{dQ_1^{(a)}}{ds} = 0, \quad \frac{dM_1^{(a)}}{ds} + B\frac{h}{2}\tau - Q_1^{(a)} = 0,\\
&\frac{d\tau}{ds} = -\frac{2k_x}{B}\left(\frac{N_1^{(a)}}{A_1} + \frac{h}{2}\frac{M_1^{(a)}}{D_1}\right),
\end{aligned}
\tag{38}
$$

within intervals OB and BC. From Eqs. (37) it is a straightforward matter to obtain the internal forces in interval AO,

$$
N_1^{(a)} = A_4, \quad Q_1^{(a)} = A_5, \quad \text{and} \quad M_1^{(a)} = A_5 s + A_6,
\tag{39}
$$

where A_4, A_5, and A_6 are integration constants. Moving on to solve Eqs. (38), we differentiate the third equation with respect to s and substitute the result into the second and fourth equations, obtaining

$$N_1^{(a)} = \frac{A_1}{k_x h} \frac{d^2 M_1^{(a)}}{ds^2} - \frac{A_1 h}{2} \frac{M_1^{(a)}}{D_1} . \tag{40}$$

Then, by substituting the first equation in (38) and Eq. (40) into the fourth equation in (38), we obtain a fourth-order differential equation,

$$\frac{d^4 M_1^{(a)}}{ds^4} - 2k_x \left(\frac{1}{A_1} + \frac{h^2}{4D_1}\right) \frac{d^2 M_1^{(a)}}{ds^2} = 0 , \tag{41}$$

for the bending moment. Its biquadratic characteristic equation,

$$\lambda^4 - 2k_x \left(\frac{1}{A_1} + \frac{h^2}{4D_1}\right) \lambda^2 = 0 , \tag{42}$$

has the following four roots:

$$\lambda_5 = \sqrt{2k_x \left(\frac{1}{A_1} + \frac{h^2}{4D_1}\right)}, \quad \lambda_6 = -\lambda_5, \quad \lambda_7 = \lambda_8 = 0 . \tag{43}$$

Thus, the bending moment can be expressed as

$$M_1^{(a)} = B_6 \cosh \lambda_5 s + B_7 \sinh \lambda_5 s + B_8 s + B_9 , \tag{44}$$

where B_6, B_7, B_8, and B_9 are integration constants. From Eqs. (40) and (44), we obtain the axial force,

$$N_1^{(a)} = \frac{2}{h} (B_6 \cosh \lambda_5 s + B_7 \sinh \lambda_5 s) - \frac{A_1 h}{2D_1} (B_8 s + B_9) . \tag{45}$$

Then, from the third of Eqs. (38) we deduce the shear force,

$$Q_1^{(a)} = \left(1 + \frac{A_1 h^2}{4D_1}\right) B_8 , \tag{46}$$

and from the first of Eqs. (38), the tangential interfacial stress,

$$\tau = -\frac{2}{Bh} \lambda_5 (B_6 \sinh \lambda_5 s + B_7 \cosh \lambda_5 s) + \frac{A_1 h}{2BD_1} B_8 . \tag{47}$$

Eqs. (44)–(47) represent the solution to Eqs. (38) in interval *OB*. The same expressions for the solution hold in interval *BC*, provided the integration constants B_6, B_7, B_8, and B_9 are replaced by C_6, C_7, C_8, and C_9, respectively.

4.3.2 Static boundary conditions

To determine the eleven unknown integration constants, the following ten boundary conditions apply:

$$\begin{aligned}
&N_1^{(a)}\Big|_{s=s_A}=0, && Q_1^{(a)}\Big|_{s=s_A}=\frac{\ell}{2L}P_{\mathrm{II}}, && M_1^{(a)}\Big|_{s=s_A}=0,\\
&N_1^{(a)}\Big|_{s=0^-}=N_1^{(a)}\Big|_{s=0^+}, && Q_1^{(a)}\Big|_{s=0^-}=Q_1^{(a)}\Big|_{s=0^+}, && M_1^{(a)}\Big|_{s=0^-}=M_1^{(a)}\Big|_{s=0^+},\\
&N_1^{(a)}\Big|_{s={s_B}^-}=N_1^{(a)}\Big|_{s={s_B}^+}, && Q_1^{(a)}\Big|_{s={s_B}^-}=Q_1^{(a)}\Big|_{s={s_B}^+}+\frac{1}{2}P_{\mathrm{II}}, && M_1^{(a)}\Big|_{s={s_B}^-}=M_1^{(a)}\Big|_{s={s_B}^+},\\
&N_1^{(a)}\Big|_{s=s_C}=0.
\end{aligned} \tag{48}$$

The missing condition is obtained by requiring continuity at section *B* of the bottom surface axial displacement, $\underline{u}_1^{(a)}=u_1^{(a)}+\phi_1^{(a)}\,h/2$ or, equivalently, continuity of the tangential interfacial stress,

$$\tau\Big|_{s={s_B}^-}=\tau\Big|_{s={s_B}^+}. \tag{49}$$

By substituting the expressions for the internal forces and interfacial stresses deduced in Section 4.3.1 into Eqs. (48) and (49), the integration constants are determined as follows:

$$\begin{aligned}
&A_4=0,\quad A_5=\frac{P_{\mathrm{II}}}{2}\frac{\ell}{L},\quad A_6=\frac{P_{\mathrm{II}}}{2}\frac{\ell}{L}a,\\
&B_6=\frac{P_{\mathrm{II}}}{2}\frac{\ell}{L}\frac{a}{1+\dfrac{4D_1}{A_1h^2}},\quad B_7=\frac{P_{\mathrm{II}}}{2}\frac{1}{1+\dfrac{4D_1}{A_1h^2}}\frac{\sinh\lambda_5\ell-\lambda_5a\dfrac{\ell}{L}\cosh\lambda_5b}{\lambda_5\sinh\lambda_5b},\\
&B_8=\frac{P_{\mathrm{II}}}{2}\frac{\ell}{L}\frac{1}{1+\dfrac{A_1h^2}{4D_1}},\quad B_9=\frac{P_{\mathrm{II}}}{2}\frac{\ell}{L}\frac{a}{1+\dfrac{A_1h^2}{4D_1}},\\
&C_6=\frac{P_{\mathrm{II}}}{2}\frac{1}{1+\dfrac{4D_1}{A_1h^2}}\frac{\sinh\lambda_5(d-a)+\lambda_5a\dfrac{\ell}{L}}{\lambda_5},
\end{aligned} \tag{50}$$

$$C_7 = -\frac{P_{\mathrm{II}}}{2}\frac{1}{1+\frac{4D_1}{A_1h^2}}\frac{\sinh\lambda_5(d-a)+\lambda_5 a\frac{\ell}{L}}{\lambda_5\sinh\lambda_5 b}\cosh\lambda_5 b,$$

$$C_8 = -\frac{P_{\mathrm{II}}}{2}\frac{d}{L}\frac{1}{1+\frac{A_1h^2}{4D_1}},\quad C_9 = \frac{P_{\mathrm{II}}}{2}\frac{d}{L}\frac{b}{1+\frac{A_1h^2}{4D_1}}.$$

4.3.3 Internal forces and interfacial stresses

By substituting the expressions for the integration constants (50) into the solution to the differential problem deduced in Section 4.3.1, we obtain the internal forces

$$N_1^{(a)} = 0,\quad Q_1^{(a)} = \frac{P_{\mathrm{II}}}{2}\frac{\ell}{L},\quad \text{and}\quad M_1^{(s)} = \frac{P_{\mathrm{II}}}{2}\frac{\ell}{L}(a+s), \tag{51}$$

within interval AO; and the internal forces and interfacial stresses

$$\begin{aligned}
N_1^{(a)} &= \frac{P_{\mathrm{II}}}{h}\frac{1}{1+\frac{4D_1}{A_1h^2}}\left[\frac{\sinh\lambda_5\ell\sinh\lambda_5 s+\lambda_5 a\frac{\ell}{L}\sinh\lambda_5(b-s)}{\lambda_5\sinh\lambda_5 b}-\frac{\ell}{L}(a+s)\right],\\
Q_1^{(a)} &= \frac{P_{\mathrm{II}}}{2}\frac{\ell}{L},\\
M_1^{(a)} &= \frac{P_{\mathrm{II}}}{2}\frac{1}{1+\frac{4D_1}{A_1h^2}}\left[\frac{\sinh\lambda_5\ell\sinh\lambda_5 s+\lambda_5 a\frac{\ell}{L}\sinh\lambda_5(b-s)}{\lambda_5\sinh\lambda_5 b}+\frac{4D_1}{A_1h^2}\frac{\ell}{L}(a+s)\right],\\
\tau &= \frac{P_{\mathrm{II}}}{Bh}\frac{1}{1+\frac{4D_1}{A_1h^2}}\left[\frac{\ell}{L}-\frac{\sinh\lambda_5\ell\cosh\lambda_5 s-\lambda_5 a\frac{\ell}{L}\cosh\lambda_5(b-s)}{\sinh\lambda_5 b}\right],
\end{aligned} \tag{52}$$

within interval OB, and

$$\begin{aligned}
N_1^{(a)} &= \frac{P_{\mathrm{II}}}{h}\frac{1}{1+\frac{4D_1}{A_1h^2}}\left\{\frac{[\sinh\lambda_5(d-a)+\lambda_5 a\frac{\ell}{L}]\sinh\lambda_5(b-s)}{\lambda_5\sinh\lambda_5 b}-\frac{d}{L}(b-s)\right\},\\
Q_1^{(a)} &= -\frac{P_{\mathrm{II}}}{2}\frac{d}{L},\\
M_1^{(a)} &= \frac{P_{\mathrm{II}}}{2}\frac{1}{1+\frac{4D_1}{A_1h^2}}\left\{\frac{[\sinh\lambda_5(d-a)+\lambda_5 a\frac{\ell}{L}]\sinh\lambda_5(b-s)}{\lambda_5\sinh\lambda_5 b}+\frac{4D_1}{A_1h^2}\frac{d}{L}(b-s)\right\},
\end{aligned} \tag{53}$$

$$\tau = -\frac{P_{\mathrm{II}}}{Bh}\frac{1}{1+\frac{4D_1}{A_1 h^2}}\{\frac{d}{L} - \frac{[\sinh\lambda_5(d-a)+\lambda_5 a\frac{\ell}{L}]\cosh\lambda_5(b-s)}{\sinh\lambda_5 b}\},$$

within interval *BC*.

4.4 Solution of the complete problem

4.4.1 Internal forces

The solution to the complete problem in terms of internal forces is obtained by superimposing the solution to the symmetric subproblem, Eqs. (35)–(36), and the solution to the antisymmetric subproblem, Eqs. (51)–(53), by means of Eqs. (14), (16), and (17). The resulting expressions are omitted here for the sake of brevity.

4.4.2 Displacements

The axial and transverse relative displacements at the interface are promptly obtained by substituting the expressions for the interfacial stresses appearing in Eqs. (36) and (52)–(53) into (5):

$$\begin{aligned}\Delta u &= \frac{P_{\mathrm{II}}h}{2BD_1}\frac{\ell}{L}\frac{1}{\lambda_5^2}[\lambda_5 a\frac{\cosh\lambda_5(b-s)}{\sinh\lambda_5 b}+1] \\ &\quad + \frac{P_{\mathrm{II}}h}{2BD_1}\frac{1}{\lambda_5^2}\cdot\begin{cases} -\frac{\sinh\lambda_5\ell\cosh\lambda_5 s}{\sinh\lambda_5 b}, & s\in[0,\,s_B], \\ [\frac{\sinh\lambda_5(b-\ell)\cosh\lambda_5(b-s)}{\sinh\lambda_5 b}-1], & s\in[s_B,\,s_C], \end{cases} \\ \Delta w &= -\frac{2P_{\mathrm{I}}}{BD_1}(\frac{b_2\cosh\lambda_1 s+b_3\sinh\lambda_1 s}{\lambda_2^2}+\frac{b_4\cosh\lambda_2 s+b_5\sinh\lambda_2 s}{\lambda_1^2}),\quad s\in[0,\,s_C],\end{aligned} \tag{54}$$

where the following relationships have been used:

$$k_x = \frac{1}{2}\frac{\lambda_5^2}{\frac{1}{A_1}+\frac{h^2}{4D_1}} \quad \text{and} \quad k_z = \frac{1}{2}\lambda_1^2\lambda_2^2 D_1. \tag{55}$$

As far as the sublaminates' displacements are concerned, the solution to the complete problem is deduced as follows. The expressions for the internal forces, obtained as explained in Section 4.4.1, are substituted into Eqs. (11) and integrated with respect to the curvilinear abscissa, *s*. Thus, we obtain

$$
\begin{aligned}
& u_1 = A_7, \\
& \phi_1 = \frac{1}{2BD_1}(P_{\mathrm{I}} + \frac{\ell}{2L}P_{\mathrm{II}})(s^2 + 2as) + A_8, \\
& w_1 = -\frac{1}{6BD_1}(P_{\mathrm{I}} + \frac{\ell}{2L}P_{\mathrm{II}})(s^3 + 3as^2) + [\frac{1}{BC_1}(P_{\mathrm{I}} + \frac{\ell}{2L}P_{\mathrm{II}}) - A_8]\, s + A_9, \\
& u_2 = A_{10}, \\
& \phi_2 = -\frac{1}{2BD_1}(P_{\mathrm{I}} - \frac{\ell}{2L}P_{\mathrm{II}})(s^2 + 2as) + A_{11}, \\
& w_2 = \frac{1}{6BD_1}(P_{\mathrm{I}} - \frac{\ell}{2L}P_{\mathrm{II}})(s^3 + 3as^2) - [\frac{1}{BC_1}(P_{\mathrm{I}} - \frac{\ell}{2L}P_{\mathrm{II}}) + A_{11}]\, s + A_{12},
\end{aligned}
\tag{56}
$$

where A_7, A_8, …, A_{12} are integration constants, within interval AO;

$$
\begin{aligned}
& u_1 = \frac{P_{\mathrm{II}}}{B}\frac{h}{A_1 h^2 + 4D_1}[\frac{\sinh\lambda_5\ell\cosh\lambda_5 s - \lambda_5 a\frac{\ell}{L}\cosh\lambda_5(b-s)}{\lambda_5^2\sinh\lambda_5 b} - \frac{1}{2}\frac{\ell}{L}(s^2 + 2as)] + B_{10}, \\
& \phi_1 = \frac{P_{\mathrm{I}}}{BD_1}(\frac{b_2\sinh\lambda_1 s + b_3\cosh\lambda_1 s}{\lambda_1} + \frac{b_4\sinh\lambda_2 s + b_5\cosh\lambda_2 s}{\lambda_2}) + \\
& \quad + \frac{P_{\mathrm{II}}}{B}\frac{1}{A_1 h^2 + 4D_1}[\frac{A_1 h^2}{2D_1}\frac{\sinh\lambda_5\ell\cosh\lambda_5 s - \lambda_5 a\frac{\ell}{L}\cosh\lambda_5(b-s)}{\lambda_5^2\sinh\lambda_5 b} + \frac{\ell}{L}(s^2 + 2as)] + B_{11}, \\
& w_1 = \frac{P_{\mathrm{I}}}{BD_1}(\frac{b_2\cosh\lambda_1 s + b_3\sinh\lambda_1 s}{\lambda_2^2} + \frac{b_4\cosh\lambda_2 s + b_5\sinh\lambda_2 s}{\lambda_1^2}) + \\
& \quad - \frac{P_{\mathrm{II}}}{B}\frac{1}{A_1 h^2 + 4D_1}[\frac{A_1 h^2}{2D_1}\frac{\sinh\lambda_5\ell\sinh\lambda_5 s + \lambda_5 a\frac{\ell}{L}\sinh\lambda_5(b-s)}{\lambda_5^3\sinh\lambda_5 b} + \frac{1}{3}\frac{\ell}{L}(s^3 + 3as^2)] + \\
& \quad + (\frac{P_{\mathrm{II}}}{2BC_1}\frac{\ell}{L} - B_{11})\, s + B_{12}, \\
& u_2 = -\frac{P_{\mathrm{II}}}{B}\frac{h}{A_1 h^2 + 4D_1}[\frac{\sinh\lambda_5\ell\cosh\lambda_5 s - \lambda_5 a\frac{\ell}{L}\cosh\lambda_5(b-s)}{\lambda_5^2\sinh\lambda_5 b} - \frac{1}{2}\frac{\ell}{L}(s^2 + 2as)] + B_{13}, \\
& \phi_2 = -\frac{P_{\mathrm{I}}}{BD_1}(\frac{b_2\sinh\lambda_1 s + b_3\cosh\lambda_1 s}{\lambda_1} + \frac{b_4\sinh\lambda_2 s + b_5\cosh\lambda_2 s}{\lambda_2}) + \\
& \quad + \frac{P_{\mathrm{II}}}{B}\frac{1}{A_1 h^2 + 4D_1}[\frac{A_1 h^2}{2D_1}\frac{\sinh\lambda_5\ell\cosh\lambda_5 s - \lambda_5 a\frac{\ell}{L}\cosh\lambda_5(b-s)}{\lambda_5^2\sinh\lambda_5 b} + \frac{\ell}{L}(s^2 + 2as)] + B_{14},
\end{aligned}
\tag{57}
$$

$$w_2 = -\frac{P_{\mathrm{I}}}{BD_1}\left(\frac{b_2\cosh\lambda_1 s + b_3\sinh\lambda_1 s}{\lambda_2^2} + \frac{b_4\cosh\lambda_2 s + b_5\sinh\lambda_2 s}{\lambda_1^2}\right) +$$
$$-\frac{P_{\mathrm{II}}}{B}\frac{1}{A_1h^2+4D_1}\left[\frac{A_1h^2}{2D_1}\frac{\sinh\lambda_5\ell\,\sinh\lambda_5 s + \lambda_5 a\frac{\ell}{L}\sinh\lambda_5(b-s)}{\lambda_5^3\sinh\lambda_5 b} + \frac{1}{3}\frac{\ell}{L}(s^3+3as^2)\right] +$$
$$+\left(\frac{P_{\mathrm{II}}}{2BC_1}\frac{\ell}{L} - B_{14}\right)s + B_{15},$$

where B_{10}, B_{11}, …, B_{15} are integration constants, within interval OB;

$$u_1 = -\frac{P_{\mathrm{II}}}{B}\frac{h}{A_1h^2+4D_1}\left[\frac{\sinh\lambda_5(d-a) + \lambda_5 a\frac{\ell}{L}}{\lambda_5^2\sinh\lambda_5 b}\cosh\lambda_5(b-s) - \frac{1}{2}\frac{d}{L}(s^2-2bs)\right] + C_{10},$$
$$\phi_1 = \frac{P_{\mathrm{I}}}{BD_1}\left(\frac{b_2\sinh\lambda_1 s + b_3\cosh\lambda_1 s}{\lambda_1} + \frac{b_4\sinh\lambda_2 s + b_5\cosh\lambda_2 s}{\lambda_2}\right) +$$
$$-\frac{P_{\mathrm{II}}}{B}\frac{1}{A_1h^2+4D_1}\left[\frac{A_1h^2}{2D_1}\frac{\sinh\lambda_5(d-a) + \lambda_5 a\frac{\ell}{L}}{\lambda_5^2\sinh\lambda_5 b}\cosh\lambda_5(b-s) + \frac{d}{L}(s^2-2bs)\right] + C_{11},$$
$$w_1 = \frac{P_{\mathrm{I}}}{BD_1}\left(\frac{b_2\cosh\lambda_1 s + b_3\sinh\lambda_1 s}{\lambda_2^2} + \frac{b_4\cosh\lambda_2 s + b_5\sinh\lambda_2 s}{\lambda_1^2}\right) +$$
$$-\frac{P_{\mathrm{II}}}{B}\frac{1}{A_1h^2+4D_1}\left[\frac{A_1h^2}{2D_1}\frac{\sinh\lambda_5(d-a) + \lambda_5 a\frac{\ell}{L}}{\lambda_5^3\sinh\lambda_5 b}\sinh\lambda_5(b-s) - \frac{1}{3}\frac{d}{L}(s^3-3bs^2)\right] +$$
$$-\left(\frac{P_{\mathrm{II}}}{2BC_1}\frac{d}{L} + C_{11}\right)s + C_{12},$$

$$u_2 = \frac{P_{\mathrm{II}}}{B}\frac{h}{A_1h^2+4D_1}\left[\frac{\sinh\lambda_5(d-a) + \lambda_5 a\frac{\ell}{L}}{\lambda_5^2\sinh\lambda_5 b}\cosh\lambda_5(b-s) - \frac{1}{2}\frac{d}{L}(s^2-2bs)\right] + C_{13},$$
$$\phi_2 = -\frac{P_{\mathrm{I}}}{BD_1}\left(\frac{b_2\sinh\lambda_1 s + b_3\cosh\lambda_1 s}{\lambda_1} + \frac{b_4\sinh\lambda_2 s + b_5\cosh\lambda_2 s}{\lambda_2}\right) +$$
$$-\frac{P_{\mathrm{II}}}{B}\frac{1}{A_1h^2+4D_1}\left[\frac{A_1h^2}{2D_1}\frac{\sinh\lambda_5(d-a) + \lambda_5 a\frac{\ell}{L}}{\lambda_5^2\sinh\lambda_5 b}\cosh\lambda_5(b-s) + \frac{d}{L}(s^2-2bs)\right] + C_{14}, \tag{58}$$
$$w_2 = -\frac{P_{\mathrm{I}}}{BD_1}\left(\frac{b_2\cosh\lambda_1 s + b_3\sinh\lambda_1 s}{\lambda_2^2} + \frac{b_4\cosh\lambda_2 s + b_5\sinh\lambda_2 s}{\lambda_1^2}\right) +$$
$$-\frac{P_{\mathrm{II}}}{B}\frac{1}{A_1h^2+4D_1}\left[\frac{A_1h^2}{2D_1}\frac{\sinh\lambda_5(d-a) + \lambda_5 a\frac{\ell}{L}}{\lambda_5^3\sinh\lambda_5 b}\sinh\lambda_5(b-s) - \frac{1}{3}\frac{d}{L}(s^3-3bs^2)\right] +$$
$$-\left(\frac{P_{\mathrm{II}}}{2BC_1}\frac{d}{L} + C_{14}\right)s + C_{15},$$

where C_{10}, C_{11}, …, C_{15} are integration constants, within interval BC.

The expressions for the displacement integration constants are determined as reported in Appendix B. In Part II of this paper [17], we will focus on the displacements of the application points of P_u and P_d,

$$\delta_\mathrm{u} = -w_1\big|_{s=s_A} \quad \text{and} \quad \delta_\mathrm{d} = w_1\big|_{s=s_B}, \tag{59}$$

respectively, which are necessary to compute the specimen's compliance.

5 Numerical example

By way of illustration, we consider the geometrical and mechanical properties of a 24-ply unidirectional carbon/PEEK (AS4/APC2) laminated specimen, tested in an experimental study by Reeder and Crews [10]. The specimen has span L = 100 mm, width B = 25.4 mm, and thickness H = 2h = 3 mm. The initial delamination length is a = 32 mm. The elastic moduli of the material are $E_x = 129\ \mathrm{GPa}$, $E_y = E_z = 10.1\ \mathrm{GPa}$, and $G_{xy} = G_{zx} = 5.5\ \mathrm{GPa}$, hence the sublaminates' extensional stiffness, shear stiffness, and bending stiffness are $A_1 = E_x h = 193500\ \mathrm{N/mm}$, $C_1 = 5\, G_{zx} h / 6 = 6875\ \mathrm{N/mm}$, and $D_1 = E_x h^3 / 12 = 36281\ \mathrm{N\,mm^2}$, respectively [68].

The values of the elastic constants of the interface have been obtained through a numerical compliance calibration strategy described in detail in Part II of this paper [17]. The strategy enables evaluation of the interface constants in such a way as to account for the localised deformation occurring at the crack tip, which in turn depends on the geometrical and mechanical properties of the considered specimen. For the problem at hand we obtain k_x = 31550 N/mm^3 and k_z = 23150 N/mm^3.

The applied load is $P = 100\ \mathrm{N}$ and the lever arms are $c = 43.7\ \mathrm{mm}$ and $d = 50.0\ \mathrm{mm}$. Neglecting the lever weight W, Eqs. (1) yield the loads applied to the specimen, $P_\mathrm{u} = 87.4\ \mathrm{N}$ and $P_\mathrm{d} = 187.4\ \mathrm{N}$. From Eqs. (2), the loads responsible for fracture modes I and II turn out to be $P_\mathrm{I} = 40.6\ \mathrm{N}$ and $P_\mathrm{II} = 187.4\ \mathrm{N}$, respectively. Hence, according to the SBT model (see Part II of this paper [17]), the mixed-mode ratio is $\alpha_\mathrm{SBT} = G_\mathrm{I}^\mathrm{SBT} / G_\mathrm{II}^\mathrm{SBT} = 1$.

Figures 8a, 8b, and 8c respectively show the axial forces, shear forces, and bending moments – computed as indicated in Section 4.4 – in the upper and lower sublaminates, as functions of the abscissa, s. From the left-hand end of the specimen ($s = s_A = -32$ mm) to the crack-tip section ($s = 0$), the internal forces show the typical trends of end-loaded cantilever beams (zero axial forces, constant shear forces, and linear bending moments). From the crack-tip section on, the axial forces attain non-zero values, and the shear forces suddenly rise to peak values and then decay. At the downward load application point ($s = s_B = 18$ mm), the shear forces are discontinuous and the bending moments exhibit cusps. Afterwards, approaching the right-hand end of the specimen ($s = s_C = 68$ mm), the internal forces nearly correspond to those of two perfectly bonded sublaminates behaving as a single whole.

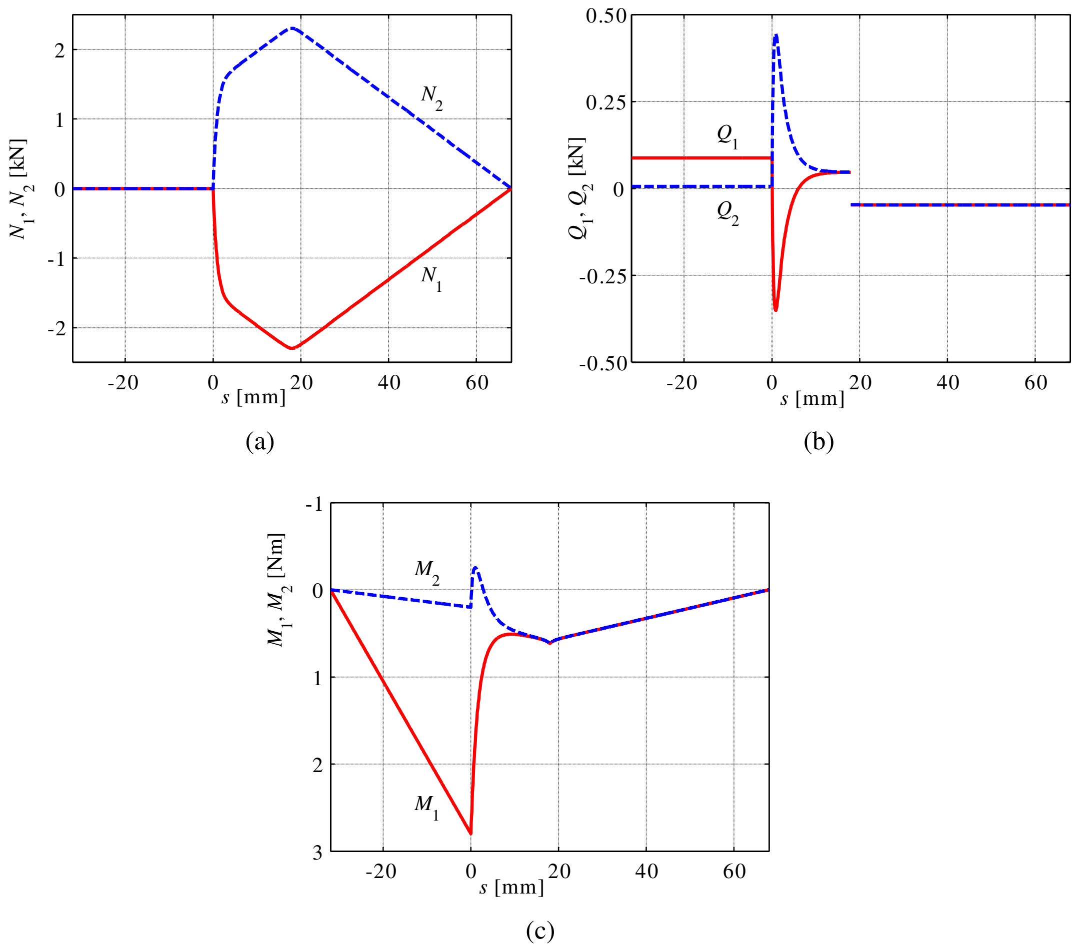

Fig. 8 Internal forces in sublaminates: (**a**) axial force; (**b**) shear force; (**c**) bending moment

Figures 9a and 9b respectively show the normal and tangential interfacial stresses – computed via their expressions appearing in Eqs. (36) and (52)–(53) – as functions of the abscissa, s. Both stress components attain peak values at the crack tip ($s = 0$). The normal stress decays within a short distance, exhibiting oscillations of decreasing, negligible amplitude. The tangential stress, except for narrow regions around the crack tip and the downward load application point ($s = s_B = 18$ mm), is approximately equal to the values predicted by Jourawski's formula for unbroken cross sections on intervals OB and BC,

$$\tau_{OB} \cong \frac{P_{II}}{Bh} \frac{1}{1+\dfrac{4D_1}{A_1 h^2}} \frac{\ell}{L} = 1.84 \text{ MPa} \quad \text{and} \quad \tau_{BC} \cong -\frac{P_{II}}{Bh} \frac{1}{1+\dfrac{4D_1}{A_1 h^2}} \frac{d}{L} = -1.84 \text{ MPa}. \tag{60}$$

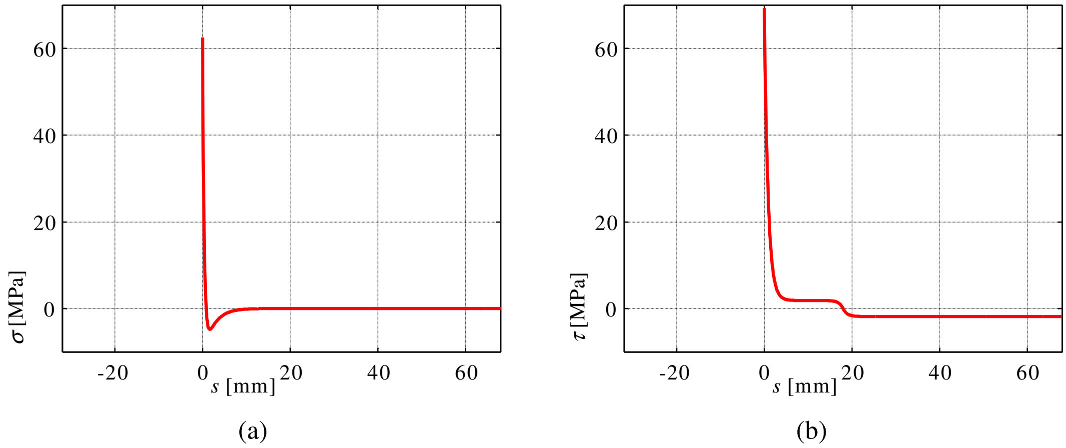

Fig. 9 Interfacial stresses: (**a**) normal stress; (**b**) tangential stress

Figures 10a, 10b, and 10c respectively show the axial displacements, transverse displacements, and cross-sections' rotations – computed via Eqs. (56)–(58) – in the upper and lower sublaminates, as functions of the abscissa, s. From the left-hand end of the specimen to the crack-tip section, the displacements show the typical trends of end-loaded cantilever beams. In the regions bonded by the interface, except for a limited neighbourhood around the crack-tip, the displacements nearly correspond to those of two perfectly bonded sublaminates behaving as a single whole. As can be noticed, the EBT model predicts significant relative rotation between the sublaminates' cross sections at the crack tip (Fig. 10c). This relative rotation is related to the so-called 'root rotations' of the sublaminates, which have often been noted in the literature [19, 30, 71, 72] as one of the main features to be taken into account by models aiming to accurately evaluate a specimen's compliance and energy release rate.

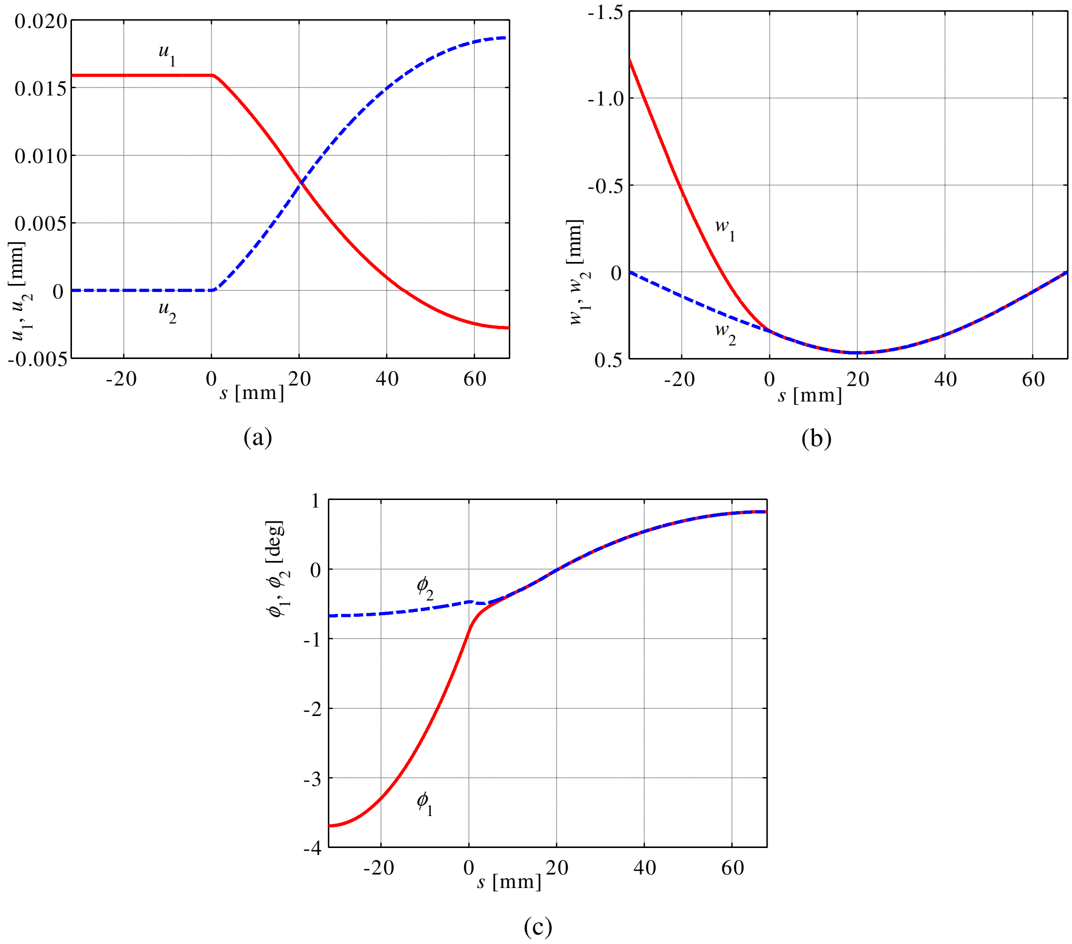

Fig. 10 Displacements of sublaminates: (**a**) axial displacement; (**b**) transverse displacement; (**c**) cross-section rotation

6 Conclusions

An enhanced beam-theory model of the MMB test has been developed, wherein the laminated specimen is considered as an assemblage of two sublaminates – modelled as extensible, flexible, and shear-deformable beams – partly connected by an elastic–brittle interface. A complete explicit solution to the problem has been deduced, including analytical expressions for the internal forces, interfacial stresses, and displacements.

Based on the solution obtained, any mechanical quantity of interest can be computed, thus allowing parametric studies and comparisons with theoretical and experimental results to be performed. In particular, in Part II of this paper [17] analytical expressions will be deduced for the compliance, energy release rate, and mode mixity. Comparisons with analytical models reported in the literature and finite element analyses will also be presented.

The deformable interface connecting the sublaminates enables the enhanced beam-theory model to account for the localised deformation occurring at the crack tip, including the so-called 'root rotations' frequently evoked in the literature to explain discrepancies between the predictions of the simple beam-theory model and experimental and numerical results [19, 30, 71, 72].

The solution strategy adopted is to decompose the problem into two subproblems related to the symmetric and antisymmetric parts of the loads. Through this decomposition, it has been demonstrated that the symmetric and antisymmetric load systems are responsible for the normal and tangential interfacial stresses, respectively, so that they correspond to pure fracture modes I and II. Actually, the symmetric and antisymmetric load systems can be regarded as those corresponding to DCB and ENF tests, respectively. Although the abovementioned load decomposition is always permissible for linear models, it should be noted that it furnishes correct partitioning of fracture modes only for symmetric specimens. Unfortunately, with few exceptions [39, 41], this point appears not to have been fully appreciated in the literature [22–24, 36–38, 45–49].

In conclusion, we would like to emphasise that the solution obtained holds not only for homogeneous orthotropic specimens, but also for unidirectional and multidirectional laminated specimens, as well as adhesively bonded specimens. This represents a strong point of the model and a novelty with respect to similar models available in the literature.

Appendix A – Boundary conditions for the overall problem

The boundary conditions for the overall problem are obtained by considering the static and kinematic conditions of the specimen at sections *A*, *O*, *B*, and *C*.

At section *A* ($s = s_A = -a$) the upper sublaminate is subjected to the upward load, P_u, while the lower sublaminate is constrained by a fixed hinge:

$$\begin{aligned} &N_1\big|_{s=s_A} = 0, \quad Q_1\big|_{s=s_A} = P_\mathrm{u}, \quad M_1\big|_{s=s_A} = 0, \\ &u_2\big|_{s=s_A} = 0, \quad w_2\big|_{s=s_A} = 0, \quad M_2\big|_{s=s_A} = 0. \end{aligned} \tag{A1}$$

At section *O* ($s = 0$) the internal forces and displacements are continuous:

$$
\begin{aligned}
&N_1\big|_{s=0^-} = N_1\big|_{s=0^+}, \quad Q_1\big|_{s=0^-} = Q_1\big|_{s=0^+}, \quad M_1\big|_{s=0^-} = M_1\big|_{s=0^+}, \\
&u_1\big|_{s=0^-} = u_1\big|_{s=0^+}, \quad w_1\big|_{s=0^-} = w_1\big|_{s=0^+}, \quad \phi_1\big|_{s=0^-} = \phi_1\big|_{s=0^+}, \\
&N_2\big|_{s=0^-} = N_2\big|_{s=0^+}, \quad Q_2\big|_{s=0^-} = Q_2\big|_{s=0^+}, \quad M_2\big|_{s=0^-} = M_2\big|_{s=0^+}, \\
&u_2\big|_{s=0^-} = u_2\big|_{s=0^+}, \quad w_2\big|_{s=0^-} = w_2\big|_{s=0^+}, \quad \phi_2\big|_{s=0^-} = \phi_2\big|_{s=0^+}.
\end{aligned}
\tag{A2}
$$

At section B ($s = s_B = d - a$) the internal forces and displacements are continuous, except for the introduction of the downward load, P_d, in the upper sublaminate:

$$
\begin{aligned}
&N_1\big|_{s=s_B^-} = N_1\big|_{s=s_B^+}, \quad Q_1\big|_{s=s_B^-} = Q_1\big|_{s=s_B^+} + P_\mathrm{d}, \quad M_1\big|_{s=s_B^-} = M_1\big|_{s=s_B^+}, \\
&u_1\big|_{s=s_B^-} = u_1\big|_{s=s_B^+}, \quad w_1\big|_{s=s_B^-} = w_1\big|_{s=s_B^+}, \quad \phi_1\big|_{s=s_B^-} = \phi_1\big|_{s=s_B^+}, \\
&N_2\big|_{s=s_B^-} = N_2\big|_{s=s_B^+}, \quad Q_2\big|_{s=s_B^-} = Q_2\big|_{s=s_B^+}, \quad M_2\big|_{s=s_B^-} = M_2\big|_{s=s_B^+}, \\
&u_2\big|_{s=s_B^-} = u_2\big|_{s=s_B^+}, \quad w_2\big|_{s=s_B^-} = w_2\big|_{s=s_B^+}, \quad \phi_2\big|_{s=s_B^-} = \phi_2\big|_{s=s_B^+}.
\end{aligned}
\tag{A3}
$$

At section C ($s = s_C = L - a$) the upper sublaminate is load-free, while the lower sublaminate is simply supported:

$$
\begin{aligned}
&N_1\big|_{s=s_C} = 0, \quad Q_1\big|_{s=s_C} = 0, \quad M_1\big|_{s=s_C} = 0, \\
&N_2\big|_{s=s_C} = 0, \quad w_2\big|_{s=s_C} = 0, \quad M_2\big|_{s=s_C} = 0.
\end{aligned}
\tag{A4}
$$

Appendix B – Displacement integration constants

By expressing the kinematic boundary conditions contained in Eqs. (A1)–(A4) in terms of the displacements (56)–(58), we obtain 15 linear equations. Three further conditions are obtained by substituting Eqs. (57) and (58) into Eqs. (7) and making the resulting expressions equal to Eqs. (30) and (47). After some simplifications, omitted here for brevity, a set of 18 linear equations is composed, whose solution leads to the following expressions for the displacement integration constants:

$$
\begin{aligned}
B_{11} &= \frac{P_{\mathrm{I}}}{BLD_1}\Big[\frac{b_2}{\lambda_2^2}+\frac{b_4}{\lambda_1^2}+a\Big(\frac{b_3}{\lambda_2}+\frac{b_5}{\lambda_2}\Big)-\frac{b_2\cosh\lambda_1 b+b_3\sinh\lambda_1 b}{\lambda_2^2}-\frac{b_4\cosh\lambda_2 b+b_5\sinh\lambda_2 b}{\lambda_1^2}\Big]+\\
&\quad -\frac{P_{\mathrm{I}}}{BL}\Big(\frac{a^3}{3D_1}+\frac{a}{C_1}\Big)+\frac{P_{\mathrm{II}}}{BL}\Big\{\frac{a^3}{6D_1}\frac{\ell}{L}+\frac{1}{3}\frac{1}{A_1h^2+4D_1}\frac{\ell}{L}[a^2(3L-2a)-Ld(2L-d)]+\\
&\quad -\frac{1}{2L\lambda_5^2 D_1}\frac{A_1h^2}{A_1h^2+4D_1}\Big(\frac{L\sinh\lambda_5\ell-\lambda_5 a\ell\cosh\lambda_5 b}{\sinh\lambda_5 b}a+\ell b\Big)\Big\},\\
B_{12} &= bB_{11}+\frac{P_{\mathrm{I}}}{BD_1}\Big(\frac{b_2\cosh\lambda_1 b+b_3\sinh\lambda_1 b}{\lambda_2^2}+\frac{b_4\cosh\lambda_2 b+b_5\sinh\lambda_2 b}{\lambda_1^2}\Big)+\\
&\quad +\frac{P_{\mathrm{II}}}{B}\ell\Big\{\frac{a}{2C_1}\frac{1}{L}+\frac{1}{A_1h^2+4D_1}\Big[\frac{b^2(L+2a)}{3L}-\frac{\ell^2}{3}+\frac{A_1h^2}{2\lambda_5^2 D_1}\Big]\Big\},\\
B_{13} &= \frac{P_{\mathrm{II}}}{B}\frac{h}{A_1h^2+4D_1}\frac{L\sinh\lambda_5\ell-\lambda_5 a\ell\cosh\lambda_5 b}{L\lambda_5^2\sinh\lambda_5 b},\\
B_{10} &= -hB_{11}+B_{13}-\frac{P_{\mathrm{II}}}{2BD_1}\frac{h}{\lambda_5^2}\frac{\ell}{L},\\
B_{14} &= B_{11},\\
B_{15} &= B_{12},\\
A_7 &= B_{10}+\frac{P_{\mathrm{II}}}{B}\frac{h}{A_1h^2+4D_1}\frac{L\sinh\lambda_5\ell-\lambda_5 a\ell\cosh\lambda_5 b}{\lambda_5^2 L\sinh\lambda_5 b},\\
A_8 &= B_{11}+\frac{P_{\mathrm{I}}}{BD_1}\Big(\frac{b_3}{\lambda_1}+\frac{b_5}{\lambda_2}\Big)+\frac{P_{\mathrm{II}}}{2BD_1}\frac{A_1h^2}{A_1h^2+4D_1}\frac{L\sinh\lambda_5\ell-\lambda_5 a\ell\cosh\lambda_5 b}{\lambda_5^2 L\sinh\lambda_5 b},\\
A_9 &= B_{12}+\frac{P_{\mathrm{I}}}{BD_1}\Big(\frac{b_2}{\lambda_2^2}+\frac{b_4}{\lambda_1^2}\Big)-\frac{P_{\mathrm{II}}}{2BD_1}\frac{A_1h^2}{A_1h^2+4D_1}\frac{a}{\lambda_5^2}\frac{\ell}{L},\\
A_{10} &= 0,\\
A_{11} &= B_{11}-\frac{P_{\mathrm{I}}}{BD_1}\Big(\frac{b_3}{\lambda_1}+\frac{b_5}{\lambda_2}\Big)+\frac{P_{\mathrm{II}}}{2BD_1}\frac{A_1h^2}{A_1h^2+4D_1}\frac{L\sinh\lambda_5\ell-\lambda_5 a\ell\cosh\lambda_5 b}{\lambda_5^2 L\sinh\lambda_5 b},\\
A_{12} &= B_{12}-\frac{P_{\mathrm{I}}}{BD_1}\Big(\frac{b_2}{\lambda_2^2}+\frac{b_4}{\lambda_1^2}\Big)-\frac{P_{\mathrm{II}}}{2BD_1}\frac{A_1h^2}{A_1h^2+4D_1}\frac{a}{\lambda_5^2}\frac{\ell}{L},\\
C_{10} &= B_{10}+\frac{P_{\mathrm{II}}}{B}\frac{h}{A_1h^2+4D_1}\Big[\frac{1}{2}(d-a)^2+\frac{1}{\lambda_5^2}\Big],\\
C_{11} &= B_{11}-\frac{P_{\mathrm{II}}}{B}\frac{1}{A_1h^2+4D_1}\Big[(d-a)^2-\frac{A_1h^2}{2\lambda_5^2 D_1}\Big],\\
C_{12} &= B_{12}+\frac{P_{\mathrm{II}}}{B}(d-a)\Big\{\frac{1}{A_1h^2+4D_1}\Big[\frac{A_1h^2}{2\lambda_5^2 D_1}-\frac{1}{3}(d-a)^2\Big]+\frac{1}{2C_1}\Big\},\\
C_{13} &= B_{13}-\frac{P_{\mathrm{II}}}{B}\frac{h}{A_1h^2+4D_1}\Big[\frac{1}{2}(d-a)^2+\frac{1}{\lambda_5^2}\Big],\\
C_{14} &= C_{11},\\
C_{15} &= C_{12}.
\end{aligned}
\tag{B1}
$$

Acknowledgements

The financial support of the Italian Ministry of Education, University and Research (MIUR) under programme PRIN 2008 "Light structures based on multiscale material in civil engineering: stiffness and strength, assembly and industrial repeatability" (Prot. N. 20089RJKYN_002) is gratefully acknowledged.

References

1. Garg AC (1988) Delamination – A damage mode in composite structures. Eng Fract Mech 29(5):557–584. doi: http://dx.doi.org/10.1016/0013-7944(88)90181-6
2. Sela N, Ishai O (1989) Interlaminar fracture toughness and toughening of laminated composite materials: A review. Composites 20(5):423–435. doi: http://dx.doi.org/10.1016/0010-4361(89)90211-5
3. Tay TE (2003) Characterization and analysis of delamination fracture in composites: An overview of developments from 1990 to 2001. Appl Mech Rev 56(1):1–31. doi: http://dx.doi.org/10.1115/1.1504848
4. Friedrich K (editor) (1989) Application of Fracture Mechanics to Composite Materials. Elsevier, Amsterdam
5. Adams DF, Carlsson LA, Pipes RB (2003) Experimental Characterization of Advanced Composite Materials – 3rd edition. CRC Press, Boca Raton, FL
6. Brunner AJ, Blackman BRK, Davies P (2008) A status report on delamination resistance testing of polymer–matrix composites. Engng Fract Mech 75(9):2779–2794. doi: http://dx.doi.org/10.1016/j.engfracmech.2007.03.012
7. Crews JH Jr, Reeder JR (1988) A mixed-mode bending apparatus for delamination testing. NASA TM-100662. URL http://ntrs.nasa.gov/archive/nasa/casi.ntrs.nasa.gov/19890001574_1989001574.pdf
8. Reeder JR, Crews JH Jr (1990) Mixed-mode bending method for delamination testing. AIAA J 28(7):1270–1276. doi: http://dx.doi.org/10.2514/3.25204
9. Reeder JR, Crews JH Jr (1991) Nonlinear analysis and redesign of the mixed-mode bending delamination test. NASA TM-102777. URL http://ntrs.nasa.gov/archive/nasa/casi.ntrs.nasa.gov/19910010169_1991010169.pdf
10. Reeder JR, Crews JH Jr (1992) Redesign of the mixed-mode bending delamination test to reduce nonlinear effects. J Compos Tech Res 14(1):12–19. doi: http://dx.doi.org/10.1520/CTR10078J
11. Reeder JR (1992) An evaluation of mixed-mode delamination failure criteria. NASA TM-104210. URL http://ntrs.nasa.gov/archive/nasa/casi.ntrs.nasa.gov/19920009705_1992009705.pdf
12. Reeder JR (2003) Refinements to the mixed-mode bending test for delamination toughness. J Compos Tech Res 25(4):191–195. doi: http://dx.doi.org/10.1520/CTR10961J

13. ASTM (2006) Standard Test Method for Mixed Mode I-Mode II Interlaminar Fracture Toughness of Unidirectional Fiber Polymer Matrix Composites, D6671/D6671M-06. American Society for Testing and Materials, West Conshohocken, PA. doi: http://dx.doi.org/10.1520/D6671_D6671M-06
14. Allix O, Ladevèze P (1992) Interlaminar interface modelling for the prediction of delamination. Compos Struct 22(4):235–242. doi: http://dx.doi.org/10.1016/0263-8223(92)90060-P
15. Corigliano A (1993) Formulation, identification and use of interface models in the numerical analysis of composite delamination. Int J Solids Struct 30(20):2779–2811. doi: http://dx.doi.org/10.1016/0020-7683(93)90154-Y
16. Bennati S, Colleluori M, Corigliano D, Valvo PS (2009) An enhanced beam-theory model of the asymmetric double cantilever beam (ADCB) test for composite laminates. Compos Sci Technol 69(11–12):1735–1745. doi: http://dx.doi.org/10.1016/j.compscitech.2009.01.019
17. Bennati S, Fisicaro P, Valvo PS (2013) An enhanced beam-theory model of the mixed-mode bending (MMB) test – Part II: applications and results. Meccanica 48(2):465–484. doi: http://dx.doi.org/10.1007/s11012-012-9682-7
18. Chen JH, Sernow R, Schultz E, Hinrichsen G (1999) A modification of the mixed-mode bending test apparatus. Compos Part A-Appl S 30(7):871–877. doi: http://dx.doi.org/10.1016/S1359-835X(98)00193-6
19. Kinloch AJ, Wang Y, Williams JG, Yayla P (1993) The mixed-mode delamination of fibre composite materials. Compos Sci Technol 47(3):225–237. doi: http://dx.doi.org/10.1016/0266-3538(93)90031-B
20. Kenane M, Benzeggagh ML (1997) Mixed-mode delamination fracture toughness of unidirectional glass/epoxy composites under fatigue loading. Compos Sci Technol 57(5):597–605. doi: http://dx.doi.org/10.1016/S0266-3538(97)00021-3
21. Yum Y-J, You H (2001) Pure mode I, II and mixed mode interlaminar fracture of graphite/epoxy composite materials. J Reinf Plast Compos 20(9):794–808. doi: http://dx.doi.org/10.1177/073168401772678571
22. Soboyejo WO, Lu G-Y, Chengalva S, Zhang J, Kenner V (1999) A modified mixed-mode bending specimen for the interfacial fracture testing of dissimilar materials. Fatigue Fract Eng M 22(9):799–810. doi: http://dx.doi.org/10.1046/j.1460-2695.1999.00203.x
23. Marannano GV, Pasta A (2007) An analysis of interface delamination mechanisms in orthotropic and hybrid fiber-metal composite laminates. Engng Fract Mech 74(4):612–626. doi: http://dx.doi.org/10.1016/j.engfracmech.2006.09.004
24. Suárez JC, López F, Miguel S, Pinilla P, Herreros MA (2009) Determination of the mixed-mode fracture energy of elastomeric structural adhesives: evaluation of debonding buckling in fibre-metal hybrid laminates. Fatigue Fract Engng Mater Struct 32(2):127–140. doi: http://dx.doi.org/10.1111/j.1460-2695.2008.01317.x
25. Bhashyan S, Davidson BD (1997) Evaluation of data reduction methods for the mixed mode bending test. AIAA J 35(3):546–552. doi: http://dx.doi.org/10.2514/2.129

26. Kanninen MF (1973) An augmented double cantilever beam model for studying crack propagation and arrest. Int J Fract 9(1):83–92. doi: http://dx.doi.org/10.1007/BF00035958
27. Carlsson LA, Gillespie JW, Pipes RB (1986) On the analysis and design of the end notched flexure (ENF) specimen for Mode II testing. J Compos Mater 20(6):594–604. doi: http://dx.doi.org/10.1177/002199838602000606
28. Fan C, Ben Jar P-Y, Cheng J-JR (2006) Revisit the analysis of end-notched-flexure (ENF) specimen. Compos Sci Technol 66(10):1497–1498. doi: http://dx.doi.org/10.1016/j.compscitech.2006.01.016
29. Valvo PS (2008) Does shear deformability influence the mode II delamination of laminated beams?. In: ECF 17 – 17th European Conference on Fracture. 2–5 September 2008, Brno, Czech Republic
30. Williams JG (1989) End corrections for orthotropic DCB specimens. Compos Sci Technol 35(4):367–376. doi: http://dx.doi.org/10.1016/0266-3538(89)90058-4
31. Hashemi S, Kinloch AJ, Williams JG (1990) The analysis of interlaminar fracture in uniaxial fibre-polymer composites. Proc R Soc Lond A 427(1872):173–199. doi: http://dx.doi.org/10.1098/rspa.1990.0007
32. Wang Y, Williams JG (1992) Corrections for mode II fracture toughness specimens of composites materials. Compos Sci Technol 43(3):251–256. doi: http://dx.doi.org/10.1016/0266-3538(92)90096-L
33. Wang JL, Qiao PZ (2004) Novel beam analysis of end notched flexure specimen for mode-II fracture. Engrg Fract Mech 71(2):219–231. doi: http://dx.doi.org/10.1016/S0013-7944(03)00096-1
34. de Morais AB (2011) Novel cohesive beam model for the End-Notched Flexure (ENF) specimen. Engrg Fract Mech 78(17):3017–3029. doi: http://dx.doi.org/10.1016/j.engfracmech.2011.08.019
35. Jumel J, Budzik MK, Ben Salem N, Shanahan MER (2013) Instrumented End Notched Flexure – Crack propagation and process zone monitoring. Part I: Modelling and analysis. Int J Solids Struct 50(2):310–319. doi: http://dx.doi.org/10.1016/j.ijsolstr.2012.08.028
36. de Morais AB, Pereira AB (2006) Mixed mode I + II interlaminar fracture of glass/epoxy multidirectional laminates – Part 1: Analysis. Compos Sci Technol 66(13):1889–1895. doi: http://dx.doi.org/10.1016/j.compscitech.2006.04.006
37. Pereira AB, de Morais AB (2006) Mixed mode I + II interlaminar fracture of glass/epoxy multidirectional laminates – Part 2: Experiments. Compos Sci Technol 66(13):1896–1902. doi: http://dx.doi.org/10.1016/j.compscitech.2006.04.008
38. de Morais AB, Pereira AB (2007) Interlaminar fracture of multidirectional glass/epoxy laminates under mixed-mode I + II loading. Mech Compos Mater 43(3):233–244. doi: http://dx.doi.org/10.1007/s11029-007-0023-1
39. Pereira AB, de Morais AB (2008) Mixed mode I + II interlaminar fracture of carbon/epoxy laminates. Composites Part A 39(2):322–333. doi: http://dx.doi.org/10.1016/j.compositesa.2007.10.013

40. Ducept F, Davies P, Gamby D (1997) An experimental study to validate tests used to determine mixed mode failure criteria of glass/epoxy composites. Compos Part A 28(8):719–729. doi: http://dx.doi.org/10.1016/S1359-835X(97)00012-2
41. Ducept F, Gamby D, Davies P (1999) A mixed-mode failure criterion derived from tests on symmetric and asymmetric specimens. Compos Sci Technol 59(4):609–619. doi: http://dx.doi.org/10.1016/S0266-3538(98)00105-5
42. Ducept F, Davies P, Gamby D (2000) Mixed mode failure criteria for a glass/epoxy composite and an adhesively bonded composite/composite joint. Int J Adhes Adhes 20(3):233–244. doi: http://dx.doi.org/10.1016/S0143-7496(99)00048-2
43. Benzeggagh ML, Kenane M (1996) Measurement of mixed-mode delamination fracture toughness of unidirectional glass/epoxy composites with mixed-mode bending apparatus. Compos Sci Technol 56(4):439–449. doi: http://dx.doi.org/10.1016/0266-3538(96)00005-X
44. Martin RH, Hansen PL (1997) Experimental compliance calibration for the MMB specimen. In: Composite Materials: Fatigue and Fracture (Sixth Volume), edited by Armanios EA, ASTM STP 1285:305–323. doi: http://dx.doi.org/10.1520/STP19934S
45. Ozdil F, Carlsson LA (1999) Beam analysis of angle-ply laminate mixed-mode bending specimens. Compos Sci Technol 59(6):937–945. doi: http://dx.doi.org/10.1016/S0266-3538(98)00128-6
46. Kim BW, Mayer AH (2003) Influence of fiber direction and mixed-mode ratio on delamination fracture toughness of carbon/epoxy laminates. Compos Sci Technol 63(5):695–713. doi: http://dx.doi.org/10.1016/S0266-3538(02)00258-0
47. Yokozeki T, Ogasawara T, Aoki T (2008) Correction method for evaluation of interfacial fracture toughness of DCB, ENF and MMB specimens with residual thermal stresses. Compos Sci Technol 68(3-4):760–767. doi: http://dx.doi.org/10.1016/j.compscitech.2007.08.025
48. Jagan U, Chauhan PS, Parameswaran V (2008) Energy release rate for interlaminar cracks in graded laminates. Compos Sci Technol 68(6):1480–1488. doi: http://dx.doi.org/10.1016/j.compscitech.2007.10.027
49. Quispitupa A, Berggreen C, Carlsson LA (2009) On the analysis of a mixed mode bending sandwich specimen for debond fracture characterization. Engng Fract Mech 76(4):594–613. doi: http://dx.doi.org/10.1016/j.engfracmech.2008.12.008
50. Allix O, Corigliano A (1996) Modeling and simulation of crack propagation in mixed-modes interlaminar fracture specimens. Int J Fract 77(2):111–140. doi: http://dx.doi.org/10.1007/BF00037233
51. Miravete A, Jiménez MA (2002) Application of the finite element method to prediction of onset of delamination growth. Appl Mech Rev 55(2):89–105. doi: http://dx.doi.org/10.1115/1.1450763
52. Jiménez MA, Miravete A (2004) Application of the finite-element method to predict the onset of delamination growth. J Compos Mater 38(15):1309–1335. doi: http://dx.doi.org/10.1177/0021998304042734

53. Camanho PP, Dávila CG, de Moura NF (2003) Numerical simulation of mixed-mode progressive delamination in composite materials. J Compos Mater 37(16):1415–1438. doi: http://dx.doi.org/10.1177/0021998303034505
54. Turon A, Camanho PP, Costa J, Dávila CG (2006) A damage model for the simulation of delamination in advanced composites under variable-mode loading. Mech Mater 38(11):1072–1089. doi: http://dx.doi.org/10.1016/j.mechmat.2005.10.003
55. Tumino D, Cappello F (2007) Simulation of fatigue delamination growth in composites with different mode mixtures. J Compos Mater 41(20):2415–2441. doi: http://dx.doi.org/10.1177/0021998307075439
56. Oliveira JMQ, de Moura MFSF, Silva MAL, Morais JJL (2007) Numerical analysis of the MMB test for mixed-mode I/II wood fracture. Compos Sci Technol 67(2):1764–1771. doi: http://dx.doi.org/10.1016/j.compscitech.2006.11.007
57. de Moura MFSF, Oliveira JMQ, Morais JJL, Xavier J (2010) Mixed-mode I/II wood fracture characterization using the mixed-mode bending test. Engng Fract Mech 77(1):144–152. doi: http://dx.doi.org/10.1016/j.engfracmech.2009.09.014
58. Warrior NA, Pickett AK, Lourenço NSF (2003) Mixed-mode delamination – Experimental and numerical studies. Strain 39(4):153–159. doi: http://dx.doi.org/10.1046/j.1475-1305.2003.00088.x
59. Iannucci L (2006) Dynamic delamination modelling using interface elements. Comput Struct 84(15-16):1029–1048. doi: http://dx.doi.org/10.1016/j.compstruc.2006.02.002
60. Borg R, Nilsson L, Simonsson K (2004) Simulating DCB, ENF and MMB experiments using shell elements and a cohesive zone model. Compos Sci Technol 64(2):269–278. doi: http://dx.doi.org/10.1016/S0266-3538(03)00255-0
61. Aymerich F, Lecca G, Priolo P (2007) Modelling of delamination growth in composite laminates by the virtual internal bond method. Compos Part A 39(2):145–153. doi: http://dx.doi.org/10.1016/j.compositesa.2007.11.012
62. van der Meer FP, Sluys LJ (2009) A phantom node formulation with mixed mode cohesive law for splitting in laminates. Int J Fract 158(2):107–124. doi: http://dx.doi.org/10.1007/s10704-009-9344-5
63. Blanco N, Turon A, Costa J (2006) An exact solution for the determination of the mode mixture in the mixed-mode bending delamination test. Compos Sci Technol 66(10):1256–1258. doi: http://dx.doi.org/10.1016/j.compscitech.2005.10.028
64. Tenchev RT, Falzon BG (2007) A correction to the analytical solution of the mixed-mode bending (MMB) problem. Compos Sci Technol 67(3-4), 662–668. doi: http://dx.doi.org/10.1016/j.compscitech.2006.05.007
65. Massabò R, Cox BN (2001) Unusual characteristics of mixed-mode delamination fracture in the presence of large-scale bridging. Mech Compos Mat Struct 8(1):61–80. doi: http://dx.doi.org/10.1080/107594101459833
66. Szekrényes A, Uj J (2006) Comparison of some improved solutions for mixed-mode composite delamination coupons. Compos Struct 72(3):321–329. doi: http://dx.doi.org/10.1016/j.compstruct.2005.01.002

67. Szekrényes A (2007) Improved analysis of unidirectional composite delamination specimens. Mech Mat 39(10):953–974. doi: http://dx.doi.org/10.1016/j.mechmat.2007.04.002
68. Jones RM (1999) Mechanics of composite materials – 2nd edition. Taylor & Francis Inc., Philadelphia, PA
69. Vannucci P, Verchery G (2001) A special class of uncoupled and quasi-homogeneous laminates. Compos Sci Technol 61(10):1465–1473. doi: http://dx.doi.org/10.1016/S0266-3538(01)00039-2
70. Timoshenko SP (1984) Strength of materials: Elementary Theory and Problems – Vol. 1. Krieger Publishing, Melbourne, FL
71. Cotterell B, Hbaieb K, Williams JG, Hadavinia H, Tropsa V (2006) The root rotation in double cantilever beam and peel tests. Mech Mater 38(7):571–584. doi: http://dx.doi.org/10.1016/j.mechmat.2005.11.001
72. Andrews MG, Massabò R (2007) The effects of shear and near tip deformations on energy release rate and mode mixity of edge-cracked orthotropic layers. Engng Fract Mech 74(17):2700–2720. doi: http://dx.doi.org/10.1016/j.engfracmech.2007.01.013